Ecophysiological strategy switch through development in heteroblastic species of mediterranean ecosystems – an example in the African Restionaceae

Ehmig, Merten ; Coiro, Mario ; Linder, H Peter

DOI: https://doi.org/10.1093/aob/mcy194

Ecophysiological strategy switch through development in heteroblastic species of mediterranean ecosystems

—

an example in the African Restionaceae

Merten Ehmig, Mario Coiro, H Peter Linder

Manuscript published in

Annals of Botany, Volume 123, Issue 4, 14 March 2019, Pages 611–623, https://doi.org/10.1093/aob/mcy194

Published: 22 November 2018

Abstract

Heteroblasty is a non-reversible morphological change associated with life stage change and has been linked to predictable environmental variation. It is present in several clades from mediterranean-type climates, such as African Restionaceae (restios). These have heteroblastic shoots: juvenile shoots are thin, branched and sterile (sterile shoots); adult shoots are thicker and less branched, and bear inflorescences (reproductive shoots). Ten per cent of the restios retain juvenile-like, sterile shoots as adults (neoteny). We hypothesize (1) that the two shoot types differ in ecophysiological attributes, and (2) that these shoot types (and the neoteny) are associated with different environments. We measured shoot mass per surface area (SMA), maximum photosynthetic capacity per biomass (Amass) and chlorenchyma to ground tissue ratio (CGR) of both shoot types in 14 restio species. We also calculated environmental niche overlap between neotenous and non-neotenous species using an improved multidimensional overlap function based on occurrence data, and linked shoot types with environments using a phylogenetic generalized linear model.

Sterile shoots showed higher Amass, lower SMA and higher CGR than reproductive shoots. Neotenous and non-neotenous species overlapped ecologically less than expected by chance: neotenous species favoured more mesic, non-seasonal conditions.

We associate sterile shoot morphology with acquisitive ecophysiological strategies and reproductive shoots with conservative strategies. The heteroblastic switch optimizes carbon efficiency in the juvenile phase (by sterile shoots) in the mesic post-fire conditions. The adult shoots present a compromise between a more conservative strategy favourable under harsher conditions and reproductive success. Heteroblasty in seasonally arid, oligotrophic ecosystems with predictable, fire-driven shifts in water and nutrient availability might play a role in the success of restios and other species-rich lineages in mediterranean-type ecosystems. It may represent a previously unrecognized adaptation in mediterranean clades sharing similar conditions, contributing to their ecological and taxonomic dominance.

Introduction

The economical spectrum of plants spans from acquisitive strategies, to conservative strategies (Reich 2014; Pérez-Ramos *et al.* 2012). Acquisitive strategies are commonly associated with low cost, rapid investment returning, ephemeral structures whereas conservative strategies are associated with robust, stress resistant, persistent and slow investment returning organs (Westoby and Wright 2006). These strategies are associated with environmental conditions at the global (Reich *et al.* 1997, 1999) and local scale (McGill *et al.* 2006; Pérez-Ramos *et al.* 2012), with mesic environments supporting acquisitive strategies, and harsher conditions selecting for conservative strategies. Environmental conditions that change during the lifetime of individuals can select different traits at different life stages, resulting in selection for plants able to optimise their traits via phenotypic plasticity, polymorphism or heteroblasty (Lloyd 1984; Adler and Drake 2008).

Heteroblasty, in contrast to phenotypic plasticity (including environmentally controlled heterophylly) or polymorphism, is an abrupt change in morphologic traits linked to a particular life history stage (Goebel 1889; Zotz *et al.* 2011). Furthermore, a heteroblastic phenotype switch is irreversibly pre-determined. Such a morphological switch can represent an adjustment mechanism to predictable changes in environmental conditions through the lifetime of individuals (Goebel 1889; Zotz *et al.* 2011). Heteroblasty has been linked to predictable differences between the environments of juvenile and adult plants, such as the light gradient in forests (Bauer and Bauer 1980), height-limited browsing (Day 1998), or changes in water availability (Miller *et al.* 1995). However the adaptive value of heteroblasty is not straightforward, and may differ between populations of the same species (Jordan *et al.* 2000;

Climent *et al.* 2006). Despite the many reports and descriptions of heteroblastic species and groups from various ecosystems, there is still no general theory as to its advantages. Several species-rich and ecologically important groups occurring in mediterranean-type ecosystems have been reported as heteroblastic, including species of *Eucalyptus* L'Hér. (Rao 1971) and *Acacia* Mill. (Pabón-Mora and González 2012) in Australia, *Juniperus* L. in California (Miller *et al.* 1995), pines in the Mediterranean basin (Climent *et al.* 2006, 2013), and several species of the maquis (scrub) vegetation in Oceania, e.g. New Caledonia (Burns and Dawson 2006; Mueller-Dombois and Fosberg 1998). The presence of heteroblasty in these groups could indicate that this trait emerged in response to the shared mediterranean-type climate.

The mediterranean-type climate is characterized by strong precipitation seasonality with dry summers and fires on a decadal scale (Moreno and Oechel 2012). Fires result, temporarily, in more nutrient rich conditions with higher water availability by reduced water uptake from vegetation (Stock and Lewis 1986; Mappin *et al.* 2003; Clemente *et al.* 2005; Parra and Moreno 2017). Species in fire-prone environments are adapted to burning by resprouting (Verdú 2000) and/or by having seeds that germinate after fire, with germination triggered by smoke (Brown *et al.* 2003; Crosti *et al.* 2006) . Seedlings growing in post-fire conditions may benefit from the relatively better conditions. The progressive depletion of the fire induced resources and the succession of the vegetation create a predictable temporal shift from low competition and high resource availability to a competitive, less resource available environment. The increasingly harsh conditions should lead to the selection of more conservative growth strategies. These short-term benefits of fertilization and the subsequently steep gradient of nutrient impoverishment (Bergh and Compton 2015) might be more important in nutrient poor conditions, in particular mediterranean-type climates in Australia and South Africa (Christensen 1994).

The Cape Floristic Region (CFR), with its mediterranean-type climate, is a global diversity hotspot (Myers *et al.* 2000). The environmental conditions of the CFR vary both spatially and temporally, as consequence of the topography, diverse geology, seasonality (Goldblatt and Manning 2002) and the regular fires (Kraaij and van Wilgen 2014). The combination of spatial and temporal environmental variation in the CFR makes it suitable to study trait responses within individuals to changing environmental conditions through time (i.e. heteroblasty), and test whether these responses are analogous to responses to spatial environmental variation. One of the ecological dominant clades in the CFR is the 350 species-rich African Restionaceae (Restionoideae) (Briggs and Linder 2009) (hereafter “restios”) of which all species seem to be heteroblastic (Linder *et al.* 1998; Linder and Caddick 2001). Restios occur throughout the

species-rich, heathy “fynbos” vegetation (Rebelo *et al.* 2006). About 10% of the species develop sterile shoots in their adult stage (Linder 1990, 2013; Linder and Vlok 1991) which can be interpreted as neoteny, i.e. retention of juvenile characters in the adult individuals (sensu Murphy *et al.* 2003; Brown *et al.* 2006). Here we hypothesize that heteroblasty represents a response to temporal environmental shifts from relatively mesic post fire conditions to harsher conditions in mature vegetation. Species with post-fire germination thus benefit from relatively mesic conditions with suitable acquisitive ecophysiology, and in less mesic conditions adjust by a switch to more conservative strategies. We test this hypothesis by comparing ecophysiological properties of the contrasting heteroblastic growth forms of restios, as an example of a heteroblastic mediterranean clade. We test (1) for a difference in surface area per biomass (a proxy for carbon investment), in photosynthetic capacity, and in the ratio of photosynthetic tissue versus ground tissue between juvenile and adult shoot types within individuals, in order to characterize the economic strategy of the shoots. We expect juveniles to present lower biomass per surface area, higher photosynthetic capacity per biomass, and relatively more photosynthetically active tissue compared to the adults, given the more favourable conditions following fire. Furthermore, we test (2) whether acquisitive strategies are favoured in relatively more mesic conditions by comparing their niche differences between neotenous and non-neotenous species.

Material and methods

Restios

Restio leaves are highly reduced, and the shoots are the main photosynthetic organs. The juvenile plants have highly branched, thin sterile shoots, and the adult plants have unbranched or more sparsely branched and thicker, mostly erect shoots (Linder *et al.* 1998; Linder and Caddick 2001) (Fig. 1). These shoots reach a greater height than the juvenile shoots, and bear an inflorescence in the first year, but remain green for several years after flowering (Linder and Caddick 2001). Ten percent of species in the adult stage have been reported to bear sterile shoots (morphologically similar to those on the juvenile plants) on the reproductive shoots (Linder 1990, 2013; Linder and Vlok 1991) (Figs 1 and S 2). The retention of juvenile

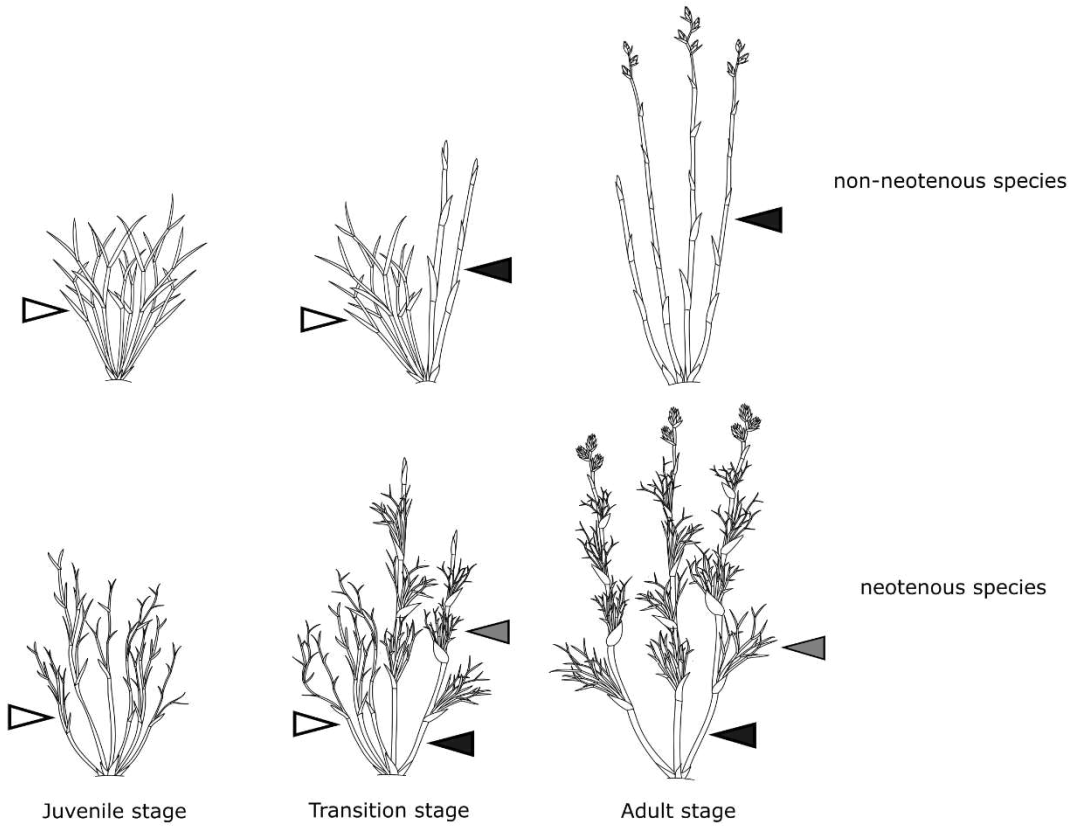

Fig. 1. Schematic drawing of idealized Restionaceae plants in different life stages, showing shoot type differences of species without shoots in adult stage (top) and neotenous species (bottom). Black arrowheads indicate reproductive shoots, grey arrowheads show adult sterile shoots in neotenous species and white arrowheads show juvenile sterile shoots.

characteristics in adult plants is described as neoteny, such as seen in heteroblastic *Acacia* (Murphy *et al.* 2003; Brown *et al.* 2006)

Data collection and analysis

For all statistical analysis we used R version 3.4.3 (R Core Team, 2016). The methods pathway is summarized and shown in Fig. 2.

Ecophysiology

Plant material

For assessing ecophysiological differences between the two shoot types (Hypothesis 1) we selected 14 species representing the major groups of restios (Table 1). Twelve species were grown from seeds, collected from natural populations by Silverhill seeds (Kenilworth, Cape Town, South Africa), in the Botanical Garden of the University of Zurich. Three species were cultivated in the Kirstenbosch National Botanical Garden. One species was present in both Zurich and Cape Town. To compare juvenile and reproductive shoots we used plants in a

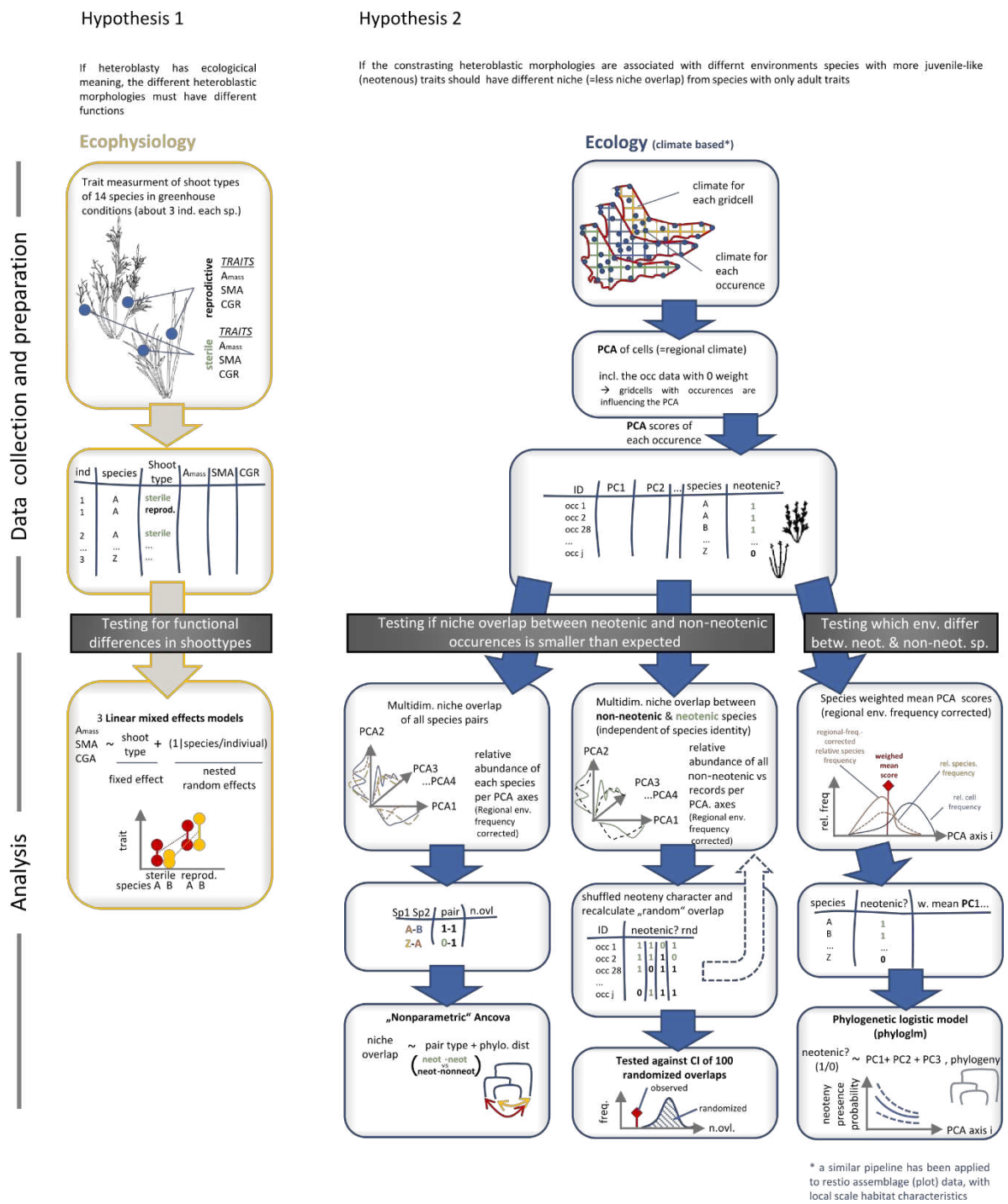

Fig. 2. Flowchart detailing the methods employed in our analyses

transition life stage (Fig. 1) where the last juvenile (sterile) shoots were still present and the first reproductive shoots had already appeared. Depending on availability of plants in the transition stage we generally used three to five plants per species, apart from two exceptions with only two and one individual per species available, for measuring shoot biomass per surface

area (SMA), photosynthetic capacity (A_{mass}) and chlorenchyma to central tissue ratio (CGR) (Table 1).

Shoot biomass per surface area

As the main photosynthetic organ in restios is the shoot, we measured SMA as an equivalent to the commonly used leaf mass per area (LMA) (Ávila-Lovera *et al.* 2017). We collected three to five shoot segments of juvenile and adult shoots per individual and scanned the projected area using an Epson Perfection 750Pro flatbed scanner with transparency mode and a resolution of 300dpi. The projected area of the samples was measured and surface area was computed using ImageJ 2.0 with the IJ-Rhizo macro (Pierret *et al.* 2013) and automatic settings. The software computes the surface area using diameter and total length, assuming a cylindrical shape. The scanned plant samples were dried for at least 72 hours at 60°C and weighed. The SMA was then calculated by dividing biomass by its respective surface area.

Photosynthetic measurements

We measured maximum photosynthetic rate for both shoot types using a Licor 6400XT Photosynthesis System (Lincoln, NB, USA) (hereafter 6400XT). All measurements were taken in climate chambers at 23 °C, 50 % humidity and about 95 $\mu Em^{-2}s^{-}\mu E$ m−2 s^{-1} light intensity. The sensor head of the 6400XT was set to 400 ppm CO2, 23 °C air temperature, and air humidity was kept within the range of 50–56 %. Measurements were taken at 2000 $\mu Em^{-2}s^{-}\mu E$ m−2 s^{-1} light intensity after visually checking for acclimatization to the highest light setting, when photosynthetic rate stopped rising (which occurred within 10 min). We programmed the 6400XT to measure photosynthetic rate for 20 s taking a measurement each second. The 6400XT is primarily designed for large leaves, and consequently air-tight sealing of the chamber for round shoots is difficult. We compensated for this by sealing the chamber with putty-like adhesives and tested for its tightness by watching for CO2 spikes when blowing air around the chamber prior to the measurements. We corrected the photosynthetic rates by the estimated half surface area of each sample, because only one side of the inserted shoot is exposed to the light source in the XT6400 measurement chamber. Area and mass for the photosynthesis samples was measured in the same way as described for the SMA measurements.

Table 1. Species of Restionaceae used for ecophysiological measurements with mean values of photosynthetic capacity (Amass) in µmol g^{-1} s^{-1}, shoot mass per surface area (SMA) in mg mm^{-2}, and the chlorenchyma to ground tissue ratio (CGR) with their standard deviation (SD) and number of individuals (n) as well as the location of the measurements taken, and voucher numbers. Values marked with asterisk* are single individual measurements.

Species	Shoot type	SMA	SD	A_{mass}	SD	n	CGR	SD	n_{CGR}	Locality	Voucher
Cannomois grandis H.P.Linder	reproductive	0.304 ±0.013	0.028	0.272 ±0.053	0.118	-5	0.125 ±0.024	0.042	-3	Zurich	ME3001
	sterile	0.070 ±0.007	0.015	1.004 ±0.173	0.387		0.643 ±0.098	0.17			
***Elegia capensis* (Burm.f.) Schelpe**	reproductive	0.077 ±0.015	0.012	1.028 ±0.225	0.318	-2	0.240 ±0.051	0.089	-3	Zurich	ME3002
	sterile	0.043 ±0.000	0.429	2.007 ±0.287	0.406		1.133 ±0.150	0.259			
Elegia equisetacea (Mast.) Mast.	reproductive	0.062 ±0.006	0.01	0.916 ±0.103	0.179		0.390 ±0.071	0.122	-3	Zurich	ME3011
	sterile	0.041 ±0.006	0.011	1.281 ±0.437	0.759		1.219 ±0.181	0.286			
***Elegia macrocarpa* (Kunth) Moline and H.P.Linder**	reproductive	0.145 ±0.009	0.145	0.631 ±0.246	0.427	-3	0.221 ±0.081	0.14	-3	Zurich	ME3003
	sterile	0.109 ±0.007	0.115	0.889 ±0.066	0.115		0.932 ±0.141	0.244			
Elegia persistens Mast.	reproductive	0.092 ±0.013	0.022	0.333 ±0.125	0.217	-3				Cape Town	
	sterile	0.047 ±0.005	0.009	0.849 ±0.230	0.398						
Restio festuciformis Nees ex Mast.	reproductive	0.123*		0.144*		-1	0.183 ±0.074	0.129	-3	Zurich	ME3004
	sterile	0.054*		0.405*			0.542 ±0.114	0.197			
Restio leptostachys Meyer	reproductive	0.099 ±0.020	0.028	0.293 ±0.015	0.021	-2	0.301 ±0.087	0.124	-2	Zurich	ME3005
	sterile	0.060 ±0.012	0.017	0.654 ±0.415	0.586		0.571 ±0.099	0.479			
Rhodocoma capensis Nees ex Steud.	reproductive	0.213 ±0.038	0.094	0.213 ±0.232	0.569	-6	0.150 ±0.050	0.08	-7	Zurich	ME3006
	sterile	0.041 ±0.003	0.007	0.041 ±0.231	0.565		1.160 ±0.181	0.479			
Rhodocoma gigantea (Kunth) H.P.Linder	reproductive	0.343 ±0.055	0.095	0.231 ±0.154	0.266	-3	0.122 ±0.024	0.053	-4	Zurich	ME3007
	sterile	0.041 ±0.005	0.009	1.016 ±0.284	0.493		0.590 ±0.114	0.228			
Thamnochortus bachmannii Mast.	reproductive	0.187 ±0.016	0.036	0.688 ±0.192	0.429	-5	0.178 ±0.024	0.333	-2	Zurich & Cape Town	ME3008
	sterile	0.064 ±0.007	0.015	0.992 ±0.299	0.668		0.985 ±0.112	0.158			
Thamnochortus cinereus.	reproductive	0.156 ±0.020	0.035	0.491 ±0.164	0.285		0.092 ±0.016	0.028		Zurich	ME3012
	sterile	0.034 ±0.004	0.006	1.562 ±0.248	0.43		1.381 ±0.033	0.057			
Thamnochortus insignis Mast.	reproductive	0.171 ±0.005	0.009	0.190 ±0.083	0.144	-3				Cape Town	
	sterile	0.063	0.014	0.164	0.84						

		±0.008		±0.485							
Thamnochortus rigidus Esterhuysen	reproductive	0.257 ±0.014	0.024	0.316 ±0.064	0.111	-3	0.312 ±0.133	0.231	-3	Zurich	ME3009
	sterile	0.051 ±0.004	0.006	0.946 ±0.240	0.416		1.045 ±0.093	0.16			
Thamnochortus spicigerus (Thunb.) Spreng.	reproductive	0.234 ±0.028	0.056	0.671 ±0.119	0.238	-4	0.261 ±0.015	0.03	-4	Zurich	ME3010
	sterile	0.070 ±0.008	0.016	1.153 ±0.155	0.31		0.884 ±0.030	0.06			

*** single individuals**

Anatomy

To explore anatomical differences between juvenile and adult shoots, we fixed juvenile and adult shoots of two to four individuals of each species in 70% EtOH (Table 1). These were hand sectioned and mounted in Hoyer's medium (Anderson 1954) according to the recipe of Coiro and Truernit (2017), photographed under fluorescence illumination using a Zeiss Axiocam HRs digital camera fitted with a Zeiss HF fluorescence filter. We measured the area of chlorenchyma and central ground tissue, which was taken to include all tissues inside the chlorenchyma, using the Circle Points method implemented in Zeiss AxioVision Version 4.8.2. We calculated the CGR of each sample.

Comparison between juvenile and adult sterile shoots in neotenous species

To test the assumption that neotenic adult sterile shoots are indeed functionally equivalent to juvenile sterile shoots, we used three neotenous species, each represented by three individuals in the transition stage (*Elegia equisetaceae*, *Rhodocoma gigantea* and *Thamnochortus cinereus*). We measured SMA, A_{mass} and CGR of adult sterile shoots, juvenile sterile shoots and reproductive shoots. The assumption of functional analogy comes from the visual similarity in architecture and general morphology and has also been described in other heteroblastic species (Murphy *et al.* 2003; Brown *et al.* 2006)

Statistical analysis

We tested for differences in SMA, A_{mass} and CGR with linear mixed effects models. SMA, A_{mass} and CGR were each used as response variables, predicted by shoot type as an explanatory variable (fixed effect) considering individual and species (nested random effects). We compared these models with models including the presence or absence of adult sterile shoots characteristic of the species (neotenous vs. non-neotenous) as a second fixed effect explanatory variable (but removing species identity from the random effects as neoteny is species-specific) to test if there are differences between neotenous and non-neotenous species.

The hypothesis that juvenile and neotenous shoots are functionally equivalent was tested by calculating the pairwise Euclidean distance in the trait-space between and within the shoot type samples within each of the three species. We were not interested in differences between species. This resulted in a data matrix of paired comparisons of shoot type for each species and the trait dissimilarity (distance) of each paired comparison. We then tested if the trait distance between neotenous and reproductive shoots is larger than the distance between neotenous and sterile shoots. We applied a linear mixed effects model of distance as the response variable predicted and the compared shoot types (e.g. 'juvenile–reproductive' comparison, 'juvenile–neotenic' comparison, 'juvenile–juvenile' comparison) as explanatory variable (fixed effect) and species identity as the random effect.

Ecology

Data acquisition

To test whether there is a niche difference between neotenous and non-neotenous species (Hypothesis 2) we scored all studied species for the presence of adult sterile shoots, based on Linder (2013). We used georeferenced occurrence data from Restionaceae assemblage plot data and herbarium records from Bolus and Compton Herbaria, assembled by H.P.L.; H.P.L. checked each record for accuracy (Fig S10).

We excluded all species that were not included in the phylogeny (Fig. S3) or had fewer than five occurrence records from the analysis. We selected annual precipitation, precipitation seasonality, precipitation in the driest month, temperature in the coldest month and in the warmest month, and temperature isothermality to reflect the climate, as these cover the range of climate variation in the CFR (Fig. S10). For each record, the environmental data were extracted from the Chelsa climate model (Karger et al., 2017). Chelsa models provide data with a grid size of 0.5 arcminutes (roughly 1 km at the equator). The regional environment was defined by a polygon surrounding the occurrence locations of all restios. We extracted environmental data for all grid cells within that polygon from the environmental models (Fig. S10)

We tested for spatial correlation between occurrences of neotenous and non-neotenous species, by first calculating the pairwise geographical distances between all individuals' locations (Euclidean distance, function dist in the stats package). We then calculated the Pearson correlation between the distance and the pairwise trait comparison matrix. An extremely small correlation of 0.0518 showed that there is no relevant spatial pattern.

Niche overlap

We performed a principal component analysis (PCA) based on the climate data extracted from all raster grid cells of the defined region and predicted PCA scores for all species occurrences in that grid cell-based (regional climate) PCA space. We used an amended method of Broennimann et al. (2012) to compute the niche overlap between neotenous and non-neotenous species based on the climatic conditions represented by the PCA scores associated with the occurrence points. We calculated Schoener's D niche overlap (Schoener, 1965) metric. The method presented by Broennimann et al. (2012) allows a comparison of binned probability densities along two environmental dimensions (here PCA axes), corrected for the regional environment abundances of two subjects (here the neotenous vs. the non-neotenous occurrences), to calculate overlap metrics. We extended the method to allow the use of more than two dimensions (see Supplementary Information S1 and Fig. S1 for details of the niche overlap calculation and method). We then constructed a null distribution of random overlaps under the assumption that neoteny state is random, by shuffling the neoteny state and computing the niche overlap between the two randomly assigned groups in 999 generated datasets. If the observed Schoener's D fell outside the upper 95 % quantile of the null distribution, we interpreted the observed niche overlap as significantly greater than the overlaps of random neotenic or non-neotenic assignment to species' occurrences.

Moreover, to account for phylogenetic relatedness between species, we calculated species pairwise niche overlaps. We then tested if niche overlap between neotenous species is smaller (neotenous species sharing more similar conditions) than niche overlap between neotenous and non-neotenous species. We used non-parametric analysis of covariance (ANCOVA), implemented in the fANCOVA package with function T.aov (Wang, 2010), using niche overlap as the response variable, the pair's neoteny states as the explanatory categorical variable (both species neotenous vs. a neotenous and non-neotenous pair) and phylogenetic distance as a numerical explanatory variable. Phylogenetic distances were calculated with the function cophenetic (Paradis et al., 2004) in the package ape using the dated restio phylogeny from Bouchenak-Khelladi and Linder (2017).

Phylogenetic logistic model

Besides niche overlap comparisons, we tested which environmental conditions may be favoured by neotenous or non-neotenous species. Based on the regional climatic PCA, we calculated mean ordination scores for each species, weighted by their relative frequency along PCA axes, which were corrected by the relative frequency of grid cells along the PCA axis –

thus, rare occurrences in conditions that are generally rare in that region have the same impact on the species mean as many occurrences in common climatic conditions. Details of the PCA are given in Fig. S5 and Tables S6–8, and the regional environment–frequency weighted-mean calculation is presented in File S2. We tested environmental effects using a phylogenetic generalized linear model (pglm) with logit link function, using the binary neoteny state (neotenous = 1, non-neotenous = 0) as the response variable, predicted by the climatic conditions represented as the mean PCA scores used as explanatory variables. We used the first three PCA axes, explaining 84.3 % of the regional variation. The model predicts a probability of presence of neotenous species (which can be understood as the probability of non-neotenic species equal to 1 − the probability of neotenous species) that theoretically translates directly into expected neotenous to non-neotenous species proportions under given environmental conditions (PCA scores).

We applied the phyloglm function implemented in the phylolm package (Ho and Ane 2014) with the IG10 method that optimizes a generalized estimating equation (GEE) approximation to the penalized likelihood of the logistic regression function. The phyloglm function incorporates the framework developed by Ives and Garland (2010). Pglms are generalized linear models implemented with a logit link function for binary response variables, and account for non-independence of closely related species, thus reducing inflated Type I errors occurring using standard methods in cases of phylogenetic conservatism (Ives and Garland 2014). The applied method uses a correlation matrix defined by a matrix formulation of the phylogenetic tree and the rate of state transitions of the species by simulated character evolution over the phylogeny. Higher transition rates make it more likely that the phylogenetic conservatism in the trait breaks, and thus can be understood as the trait being more phylogenetically independent in such a case (Ives and Garland 2010). For phylogenetic correction we used pruned trees with all species that were included in the regional climate PCA scores dataset.

We also analysed a local plot-based environmental dataset including simple moisture and soil information (Table S1) in a similar way as described using the grid cell-based climatic date for more local-scale effects (see File S3 for details about the plot-based analysis).

Furthermore, we ran two validation tests (1) to evaluate the potential of any significant results being stochastic artefacts by randomizing the neotenous species and repeating the models 999 times comparing the models' z-values to the observed model's z-value; and (2) to analyse the impact of phylogenetic uncertainty by rerunning the models on 1000 randomly sampled trees from the set of post-burnin phylogenies.

Results

Ecophysiology

Shoot mass per area

The reproductive shoots have a significantly higher SMA than juvenile sterile shoots in our sampled species ($P < 0.001$, marginal R^2=0.540, conditional R^2=0.699, Fig. 3A, Table 1 and Supplementary Data Table S1). Differences between shoot types are species-specific and range from a subtle difference of 0.02 mg mm^{-2} in *Elegia macrocarpa* to large differences such as in *Rhodocoma gigantea* with 0.3 mg mm^{-2} difference. These reflect species-specific variation in differences in shoot types, but cannot be explained by the species being neotenous or non-neotenous when using the model including species' neoteny characterization ($p_{shoot\ type} < 0.001$, $p_{neoteny} = 0.928$, marginal $R^2 = 0.552$, conditional $R^2 = 0.680$).

Maximum photosynthetic capacity per biomass

The reproductive shoots have a lower A_{mass} compared to the juvenile sterile shoots ($P < 0.001$, marginal $R^2 = 0.209$, conditional $R^2 = 0.438$), Fig. 3B, Table 1 and Supplementary Data Table S2) in all cases. The differences are species-specific, but the variation is not explained by species being neotenous or non-neotenous according to the model including neoteny character of the species ($p_{shoot\ type} < 0.001$, $p_{neoteny} = 0.457$, marginal $R^2 = 0.194$, conditional $R^2 = 0.446$). The highest differences of 0.9 µmol g^{-1} s^{-1} were observed in *Elegia capensis* and *Thamnochortus insignis* and the lowest difference of 0.25 µmol g^{-1} s^{-1} in *Restio festuciformis* and *Elegia persistens.*

Shoot anatomy

The general restio shoot anatomy agrees with previous reports (Linder 1984). Generally, sterile shoots have a higher CGR than reproductive shoots ($P < 0.001$, marginal $R^2 = 0.641$, conditional $R^2 = 0.707$, Figs 3C and 4, Table 1 and Supplementary Data Table S3). The ground tissue in the reproductive shoots has a diameter up to five times larger than in the sterile shoots,

but neotenous species do not behave significantly differently from non-neotenous species ($p_{shoot\ type} < 0.001$, $p_{neoteny} = 0.404$, marginal $R^2 = 0.645$, conditional $R^2 = 0.712$).

Neotenic adult sterile shoots

The trait distance between adult sterile shoots and reproductive shoots is significantly than that between adult sterile shoots and juvenile sterile shoots in the trait space defined by using SMA, A_{mass} and CGR ($P < 0.05$. Table 2, Supplementary Data Table S4).

Ecology

Niche overlap.

Schoener's D overlap between neotenous and non-neotenous species, calculated for the first three PC axes, was lower than the overlap distribution of the randomized trait groups ($P < 0.001$, Fig. 5). In the pairwise comparison the niche overlap between neotenous and non-neotenous species is significantly smaller ($P < 0.05$) than the within-trait (both neotenous, or both non-neotenous species compared) overlaps when testing with a non-parametric ANCOVA which included the phylogenetic distance.

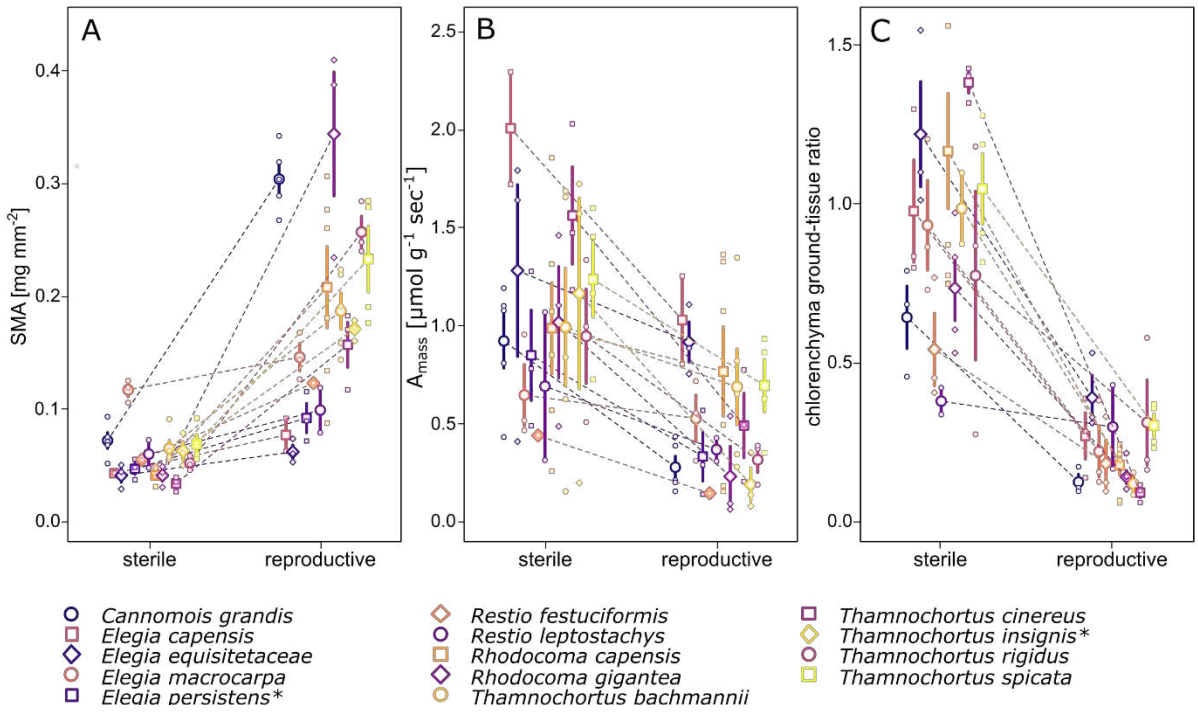

Fig. 3. Species pairwise comparison of sterile and reproductive shoots in (A) shoot mass per area (SMA), (B) maximum photosynthetic capacity(Amass) and (C) chlorenchyma to central ground tissue ratio. Large points with bar show the species' shoot type-specific mean traits with standard error, while small points represent measurement data; dashed lines link species' sterile and reproductive shoot trait means; asterisks (*) indicate species which were not included in the chlorenchyma – ground tissue ratio comparison.

Phylogenetic logistic models

The phylogenetic logistic model shows a significant relationship between PCA axes 1 (positively correlated with annual precipitation and precipitation in the driest month, explaining 40.8 % of the total variance, Tables S6–8) and 3 (negatively correlated with rainfall seasonality and positively correlated with summer drought, explaining 13.3 % of the total variance, Tables S6–8) of the regional climate PCA, and the probability of the presence of neotenous species (PCA axis 1: $P < 0.05$; PCA axis 2: $P < 0.01$, Fig. S4, Table S5). The model predicts a higher probability of neotenous species at lower values of PCA axes 1 and 3. Generally, the probability of the presence of neotenous species is low when seasonality is very high regardless of the amount of annual precipitation, and similarly when annual precipitation is low regardless of seasonality (Fig. 6 and Supplementary Data Fig. S3). The plot-based principal coordinates analysis (PCoA) (Fig. S5, Tables S9–11) also shows an increased probability of the presence of neotenous species with increasing humidity and soil fertility ($P < 0.05$, Fig. S2, Table S9).The randomization test of the trait groups shows that the z-values for the effect of PCA axes 1 and 3 are lower than the upper 95th percentile of the randomization test results (Fig. S6), showing that neotenous species are not distributed randomly across the climatic variation. P-value distributions of the topological uncertainty analysis are given in Fig. S8 for both axes, showing the robustness of the results. Similar results were obtained using the plot-based PCoA (Figs S7 and S9).

Table 2. Model coefficients of selected variables in contrast to distance between adult sterile (neotenous) shoots and sterile (juvenile) shoots of the linear mixed effects model: trait distance within species ~ shoot types compared with nested random effects of individual in species

	Estimate	**Standard error**	**Degrees of Freedom**	**t-value**	**p-value**
Intercept ($= D_{neot-sterile}$)	0.944	0.084	25.2	11.303	<0.001***
$D_{neot-repr}$		0.116	109	2.279	<0.05*
$D_{sterile-repr}$	+0.411	0.116	109	3.554	<0.001***

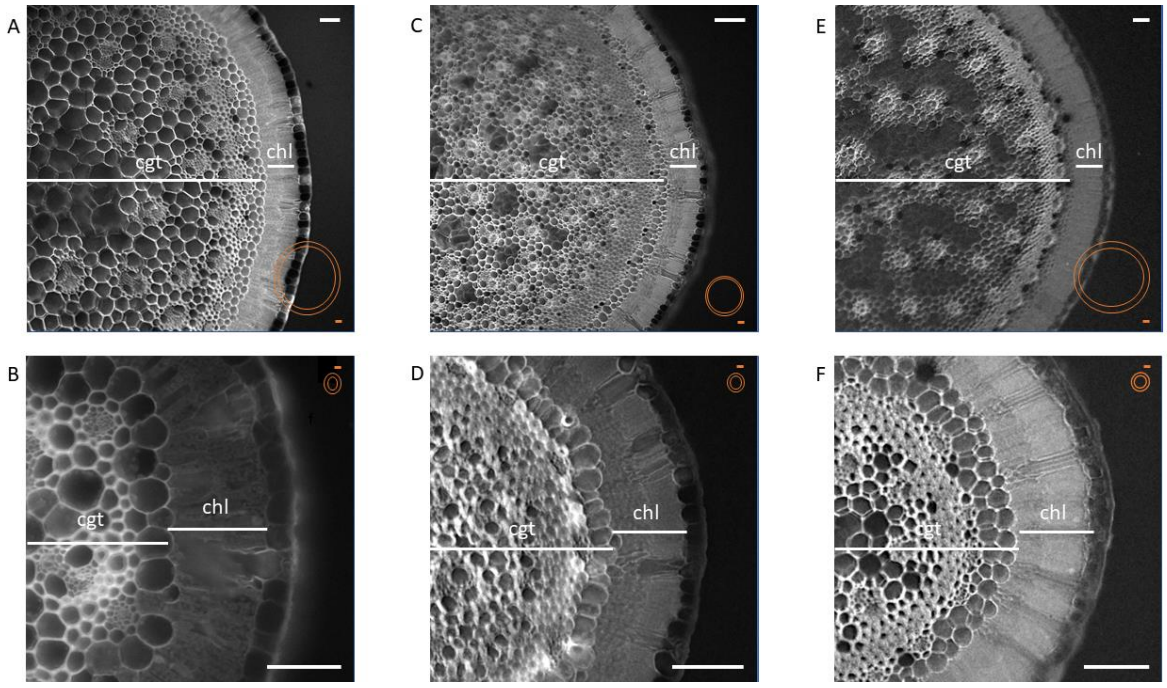

Fig. 4. Anatomy of restio shoots. The top row shows reproductive shoots and the bottom row sterile shoots, scaled to show equal shoot radius. In orange, the dimensions are visualized with equal scales. A, B, Elegia capensis; C, D, Rhodocoma capensis; E, F, Thamnochortus spicigerus. White scale bar = 100 µm; orange scale bar = 300 µm. cgt, central ground tissue; chl, chlorenchyma.

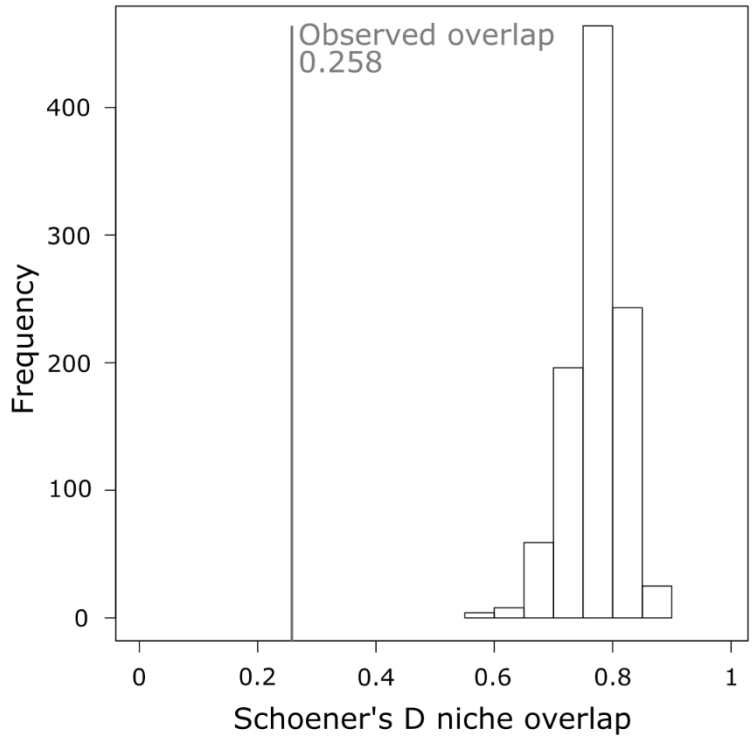

Fig. 5. Histogram of Schoener's D niche overlaps between the neotenous and non-neotenous species groups of the 999 randomized data sets with shuffled species characterization as neotenous or non-neotenous in contrast to the observed niche overlap measures in grey

Discussion

Here we show that heteroblasty in restios represents an ecophysiological transition: juvenile sterile shoots have a lower SMA and a higher A_{mass} than reproductive shoots, due to differences in the ratio of photosynthetically active and structural tissue (Figs 3 and 4). Moreover, the niche overlap between neotenous restios with adult sterile shoots and non-neotenous species is smaller than expected from random comparisons between groups of species, indicating niche differences between neotenous and non-neotenous species. Neotenous species are also more likely to be found in wetter conditions (higher annual precipitation, less seasonality, more ground moisture) and on more fertile soils (derived from shales, shale-bands or tillite, and with loamy or clayey texture) than non-neotenous species (Supplementary Data File S3 and Fig. S3). This inference corroborates our expectation that heteroblasty in mediterranean species is advantageous in habitats that experience strong environmental changes through the life cycle of the individual plants.

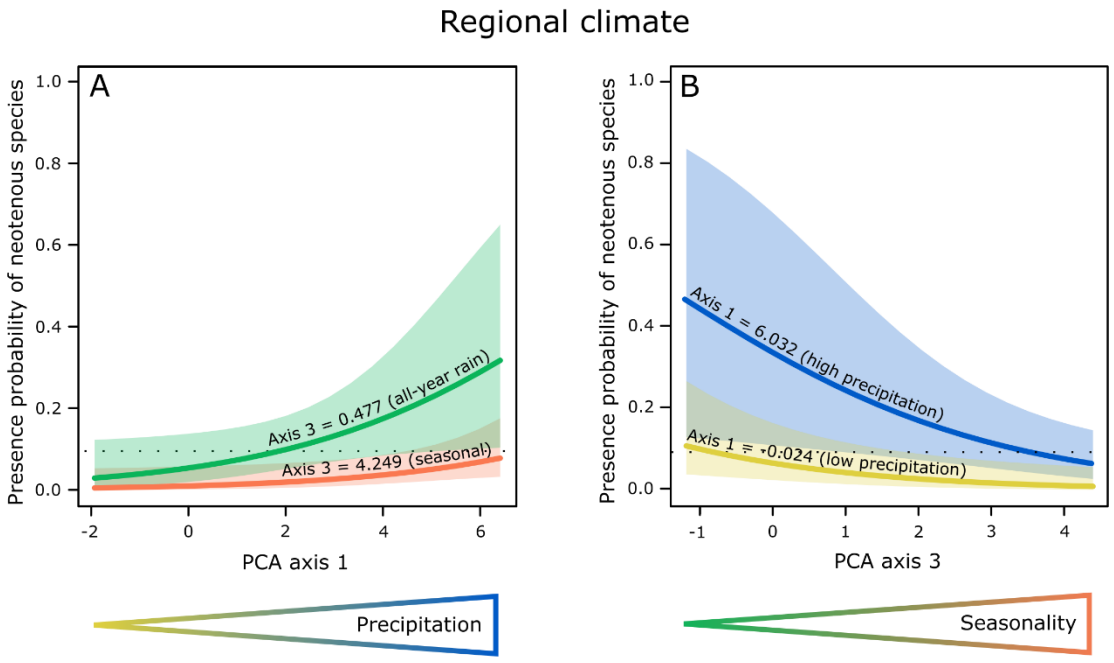

Fig. 6. Multivariate phylogenetic logistic models predicting the probability of the presence of neotenous restio species along climatic gradients represented by PCA axes based on grid-based climatic models. (A) Axis 1 correlates with precipitation and (B) axis 3 correlates with precipitation seasonality. The two curves in each graph reflect the 90th (coloured curves) and 10th (black curves) percentile values of the second significant predictor of the model. The shaded area represents the 95 % confidence intervals. The dotted line represents the expected probability of the presence of neotenous species under the null model. The non-significant predictor (axis 2) was fixed at its median.

Physiological difference of sterile and reproductive shoots

We interpret the different SMA and photosynthesis per biomass between the two shoot types as representing contrasting ecophysiological strategies. On the one hand, sterile shoots are cheap in terms of biomass per surface area, a proxy for carbon investment in leaves (Williams et al., 1989) and green stems (Ávila-Lovera et al., 2017). With higher photosynthesis rates per invested carbon, they return the invested carbon much faster than reproductive shoots. On the other hand, reproductive shoots have a slower, more conservative carbon return rate, but structurally allow for greater plant height, probably to facilitate pollination by increased pollen transfer distance (Niklas, 1985), and placing inflorescences in better wind conditions (Rosenberg et al., 1983), as well as reducing the filtration effect of the vegetation (Levin and Kerster, 1974). The combination of these factors may have a large impact at even small height differences (Handel, 1976). Taller plants may also be more effective dispersers (Thomson et al., 2018). Thus, the sterile shoot morphology may be optimal for photosynthesis, while the reproductive shoot morphology may constitute a compromise between photosynthesis, pollination, and dispersal biology. This pattern is driven largely by an allometric relationships between stem diameter and proportion of green tissue to structural tissue, representing a trade-off between photosynthesis and structural support (Boyce, 2008). The pattern we find fits the general model of the leaf economics spectrum, and its underlying anatomical basis of leaf mass per area (John et al., 2017), a key trait in the leaf economics spectrum.

Our finding of a higher SMA and lower A_{mass} in sterile shoots compared to reproductive shoots is based on measurements of plants growing in a glasshouse. We are aware that our measurements of photosynthetic rates may not represent true values under natural conditions. Nonetheless, they allowed us to compare shoot types within and between species, as conditions were kept constant for all plants, and sterile and reproductive shoots were measured sequentially on the same individual. We focused our analyses on photosynthetic rates under intense light, reflecting maximum rates, where measurement noise, overestimation due to gasket CO_2 diffusion (Pons and Welschen 2002) or internal CO_2 transport should have the least impact. In some species, and particularly for sterile shoots, we found large variance between individuals. Other than biological variability, several factors could have impacted this pattern: (1) the difficulty of using the 6400XT with multiple round samples with low surface area; (2) low readings that result in a higher impact of leaks and noise; (3) the age of the shoots which may play a role in photosynthetic responses (Makino *et al.* 1985); or (4) whole plant responses we did not account for, such as time of day (Dodd *et al.* 2005) when we placed the species in the growth chambers for measuring. Nevertheless, the general trend fits those found in SMA

and CGR and follows our expectation: we therefore believe that the differences in A_{mass} between juvenile and reproductive stages are real.

Heteroblasty as an adaptive attribute

We find that neotenous species tend to be found in different ecological conditions than non-neotenous species, suggesting that the two morphologies may have an adaptive importance. Environmental gradients, mostly studied on a spatial scale, are associated with trait changes usually resulting from changes in species composition (Pérez-Ramos *et al.* 2012). Generally, mesic conditions are linked with fast economic strategies, and harsher conditions with slow resource turnover (Reich *et al.* 1999; Wright *et al.* 2004). Our results, showing the retention of sterile shoots with their fast economics strategies in the neotenous restios under more mesic conditions, are consistent with these predictions.

Succession is commonly characterized by a shift in communities' plant traits, mediated by a temporal species turnover (Vile *et al.* 2006) or trait adjustment by species. In the early stages of succession, high growth rates and fast resource turnover may be advantageous, whereas in later stages, resource efficiency, reproduction and stress resistance gain importance (Huston and Smith 1987). Traits associated with these strategies (Wright *et al.* 2004; Pérez-Ramos *et al.* 2012; Pierce *et al.* 2016) should change accordingly, possibly driven by increasing competition. The implication is that the same species must be adapted to different, successionally separated, selective regimes.

Fire results in an increase of both total nitrogen and ammonium nitrogen just after the fire, with an increase in nitrogen in form of nitrate due to rapid nitrification of the ammonium which lasts for nine months after the fire (Stock and Lewis 1986). Fire also increases the concentration of resin-extractable phosphorus for up to 4 to 6 months after the fire, with a later mineralization phase which lasts months (Brown and Mitchell 1985). Moreover, the removal of vegetation by fire reduces evaporation of the soil-water for up to two years after fire (Scott and Wyk 1992; Mappin *et al.* 2003; Clemente *et al.* 2005; Parra and Moreno 2017), as well as reducing below-ground competition for water, which has been shown to have a significant negative effect on the growth of restio seedlings (Silvertown *et al.* 2012).

Resource availability declines in the years after fire, and below-ground competition for water and nutrients increases, thus aggravating the effects of summer drought, and leading to a harsher environment. We argue that heteroblasty in restios is an adjustment mechanism providing individuals with appropriate traits for these contrasting conditions. The high-nutrient, low below-ground competition conditions with higher water availability early in the

post-fire succession may select for the fast-economics strategy of sterile shoots, enabling the plants to invest more carbon in their rooting systems and rhizomes. This allows them to use the increased soil nitrogen available in the year after the fire by storing such nitrogen in the rhizome (Stock *et al.* 1987), as well as to reach deeper and wetter soil layers before competition and summer drought reduces available water in shallow soil horizons. The decline in water availability 2 years after fire, due to the increase in vegetation cover, and the exhaustion of the stored nutrients could promote the switch to a more conservative main tenance strategy, which increases stress resistance ability. The production of organs with higher mass per area in larger, older plants contrasts with the expected allometric relationships between age and LMA in poalean monocots, where leaves on younger plants tend to present higher LMA than leaves on older plants (reviewed in Poorter *et al.* 2009). The switch in shoot type in restios is also associated with the switch to reproduction, and so one might expect that the production of more robust shoots might be simply driven by the structural needs of bearing inflorescences (Fig. 7). However, the complete loss of juvenile shoots (and their retention in neotenous species growing in more mesic conditions) suggests that the switch to reproductive investment is not the only cause for such a heteroblastic strategy. Moreover, reproductive shoots flower only in their irst year but are maintained after flowering for years (Linder and Caddick 2001). The reproductive shoots in restios could represent a morphological adaptation that combines the advantages of a conservative economic strategy and the structural needs of reproduction.

The success of restios in the Cape flora may be partially due to their heteroblasty. With heteroblasty, plants can optimize photosynthetic efficiency in the juvenile phase, releasing carbon that can be invested in the rapid development of the rooting system, allowing the juveniles to survive the summer droughts and giving them a competitive edge in nutrient acquisition in the severely oligotrophic soils. In the adult stage, the shift in morphology to more robust, taller and more persistent shoots is functionally equivalent to being conservative with available resources and improving reproductive success. Similar ecophysiological strategy

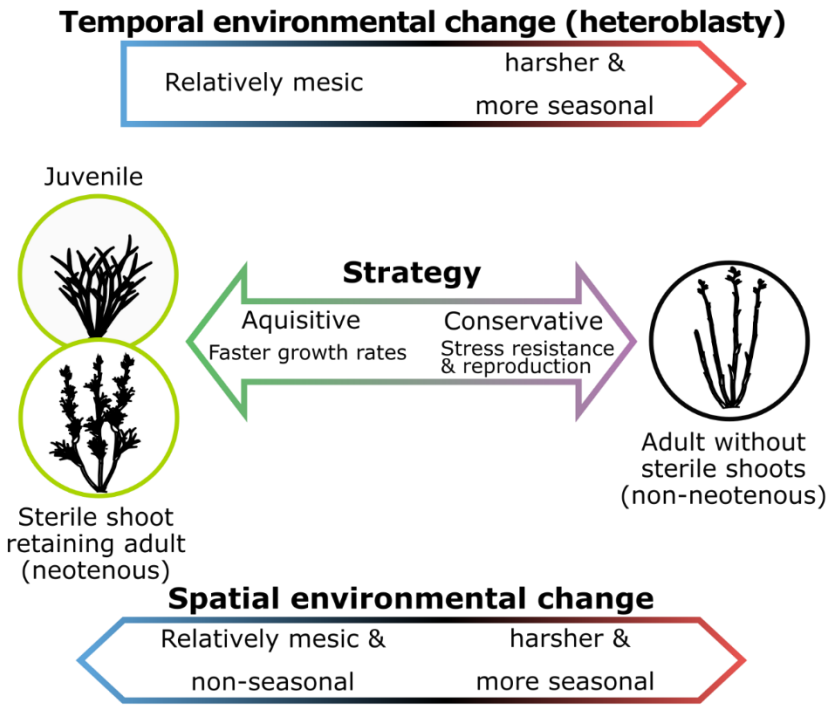

Fig. 7. Conceptual figure presenting the main results of the heteroblastic change (top) and species differences (bottom) in terms of sterile shoots linked to environmental conditions.

shifts from acquisitive to conservative have been shown in other heteroblastic groups, such as the Australian acacias (Morris *et al.* 2011), Mediterranean pines (Climent *et al.* 2006, 2013) and *Juniperus* (Miller *et al.* 1995), and might also apply to heteroblastic members of *Eucalyptus* and Australian Proteaceae. All these groups occur in seasonally dry, relatively infertile conditions with fires on a decadal scale. These fires lead to a sudden nutrient flush, followed by a decay of the nutrient addition and moisture availability together with an increase in below-ground competition during the post-fire succession. If germination is fire-triggered (so that the seedlings are found in the post-fire environment), then each plant is exposed to relatively benign conditions as a seedling, and much harsher conditions as an established plant. For heteroblasty to evolve and to persist as an advantageous mechanism, it may require long-term stable systems with periodic environmental enhancements and successive decay.

Heteroblasty as an inflexible mechanism in contrast to plasticity might cause heteroblastic species to go extinct or become displaced when the conditions for which the heteroblastic trait is advantageous disappear. However, in the restios, heteroblasty seems to have evolved at least in the common ancestor of all South African species. Therefore, heteroblasty might represent an important background trait (sensu Bouchenak-Khelladi *et al.* 2015): that is, a character that evolved before the radiation of the restios and helped to trigger the increase in diversification when the group encountered mediterranean environmental conditions. Also, in *Juniperus*,

heteroblasty potentially evolved well before the origin of *Juniperus* sect. *Sabina*, as heteroblasty is present in other Cupressaceae close to *Juniperus* (Eckenwalder 2009). The variation in the advantages of heteroblasty under differing environmental conditions in *Eucalyptus* (Jordan *et al.* 2000) provides further evidence that heteroblasty might be selected and evolve under one condition but prove be successful in other conditions as well.

We conclude that heteroblasty might present a previously unrecognized adaptation to fire-driven supra-annual flushes of nutrients and groundwater typical of mediterranean-type ecosystems.

Author contributions

M.E.; M.C. and H.P.L. wrote the paper; H.P.L. provided field data; M.E. carried out greenhouse and ecophysiology measurements; M.E. analyzed data.

Acknowledgements

We thank the members of the Linder Lab and Anna Weigand for reviewing early manuscript versions and lively discussions that improved the work, René Stalder for cultivating our plants, the ScienceCloud service of S3IT, University of Zurich, for computational support and Cape Nature for collecting permits. We also thank Ben Shipley, Kent Holsinger and two anonymous reviewers for helpful comments that greatly improved the manuscript. This work was supported by the Swiss National Science Foundation [grant number 31003A_152982 to H.P.L.] and the Claraz Schenkung. The authors have no conflict of interests to declare.

References

Adler PB, Drake JM. **2008**. Environmental Variation, Stochastic Extinction, and Competitive Coexistence. *American Naturalist* **172**: E186–E195.

Anderson LE. **1954**. Hoyer's Solution as a Rapid Permanent Mounting Medium for Bryophytes. *The Bryologist* **57**: 242–244.

Ávila-Lovera E, Zerpa AJ, Santiago LS. **2017**. Stem photosynthesis and hydraulics are coordinated in desert plant species. *New Phytologist* **216**: 1119–1129.

Bauer H, Bauer U. **1980**. Photosynthesis in leaves of the juvenile and adult phase of ivy (*Hedera helix*). *Physiologia Plantarum* **49**: 366–372.

Bergh EW, Compton JS. **2015**. A one-year post-fire record of macronutrient cycling in a mountain sandstone fynbos ecosystem, South Africa. *South African Journal of Botany* **97**: 48–58.

Bouchenak-Khelladi Y, Onstein RE, Xing Y, Schwery O, Linder HP. **2015**. On the complexity of triggering evolutionary radiations. *New Phytologist* **207**: 313–326.

Briggs B, Linder HP. **2009**. A new subfamilial and tribal classification of Restionaceae (Poales). *Telopea* **12**: 333–345.

Brown GK, Ariati SR, Murphy DJ, Miller JTH, Ladiges PY. **2006**. Bipinnate acacias (*Acacia* subg. *Phyllodineae* sect. *Botrycephalae*) of eastern Australia are polyphyletic based on DNA sequence data. *Australian Systematic Botany* **19**: 315–326.

Brown NAC, van Staden J, Daws MI, Johnson T, van Wyk AE. **2003**. Patterns in the seed germination response to smoke in plants from the Cape Floristic Region, South Africa. *South African Journal of Botany* **69**: 514–525.

Burns KC, Dawson JW. **2006**. A morphological comparison of leaf heteroblasty between New Caledonia and New Zealand. *New Zealand Journal of Botany* **44**: 387–396.

Christensen NL. **1994**. The Effects of Fire on Physical and Chemical Properties of Soils in Mediterranean-Climate Shrublands In: Ecological Studies. *The Role of Fire in Mediterranean-Type Ecosystems*. Springer, New York, NY, 79–95.

Clemente AS, Rego FC, Correia OA. **2005**. Growth, water relations and photosynthesis of seedlings and resprouts after fire. *Acta Oecologica* **27**: 233–243.

Climent J, Chambel MR, López R, Mutke S, Alía R, Gil L. **2006**. Population divergence for heteroblasty in the Canary Island pine (*Pinus canariensis*, Pinaceae). *American Journal of Botany* **93**: 840–848.

Climent J, Dantas AK, Alia R, Majada J. **2013**. Clonal variation for shoot ontogenetic heteroblasty in maritime pine (*Pinus pinaster* Ait.). *Trees* **27**: 1813–1819.

Coiro M, Truernit E. **2017**. Xylem Characterization Using Improved Pseudo-Schiff Propidium Iodide Staining of Whole Mount Samples and Confocal Laser-Scanning Microscopy In: Methods in Molecular Biology. *Xylem*. Humana Press, New York, NY, 127–132.

Crosti R, Ladd PG, Dixon KW, Piotto B. **2006**. Post-fire germination: The effect of smoke on seeds of selected species from the central Mediterranean basin. *Forest Ecology and Management* **221**: 306–312.

Day JS. **1998**. Light conditions and the evolution of heteroblasty (and the divaricate form) in New Zealand. *New Zealand Journal of Ecology* **22**: 43–54.

Dodd AN, Salathia N, Hall A, *et al.* 2005. Plant Circadian Clocks Increase Photosynthesis, Growth, Survival, and Competitive Advantage. *Science* **309**: 630–633.

Eckenwalder JE. **2009**. *Conifers of the World: The Complete Reference*. Portland: Timber Press.

Goebel K. **1889**. Über die Jugendzustände der Pflanzen. *Flora* **72**: 1–45.

Goldblatt P, Manning JC. **2002**. Plant Diversity of the Cape Region of Southern Africa. *Annals of the Missouri Botanical Garden* **89**: 281–302.

Ho LST, Ane C. **2014**. A linear-time algorithm for Gaussian and non-Gaussian trait evolution models. *Systematic Biology* **63**: 397–408.

Huston M, Smith T. **1987**. Plant Succession: Life History and Competition. *The American Naturalist* **130**: 168–198.

Ives AR, Garland T. **2010**. Phylogenetic Logistic Regression for Binary Dependent Variables. *Systematic Biology* **59**: 9–26.

Ives AR, Garland T. **2014**. Phylogenetic Regression for Binary Dependent Variables In: Garamszegi LZ, ed. *Modern Phylogenetic Comparative Methods and Their Application in Evolutionary Biology*. Berlin, Heidelberg: Springer Berlin Heidelberg, 231–261.

Jordan GJ, Potts BM, Chalmers P, Wiltshire RJE. **2000**. Quantitative genetic evidence that the timing of vegetative phase change in Eucalyptus globulus ssp. globulus is an adaptive trait. *Australian Journal of Botany* **48**: 561–567.

Kraaij T, van Wilgen BW. **2014**. Drivers, ecology, and management of fire in fynbos In: *Fynbos: ecology, evolution, and conservation of a megadiverse region*.47–72.

Linder HP. **1984**. A phylogenetic classification of the genera of the African Restionaceae. *Bothalia* **15**: 11–76.

Linder HP. **1990**. A morphological study on the *Thamnochortus erectus complex* (Restionaceae). *South African Journal of Botany* **56**: 443–449.

Linder HP. **2013**. *Delta database to Restionaceae species*. restionaceae.e-monocot.org/node/1.

Linder HP, Briggs BG, Johnson L a. S. **1998**. Restionaceae In: The Families and Genera of Vascular Plants. *Flowering Plants · Monocotyledons*. Springer, Berlin, Heidelberg, 425–445.

Linder HP, Caddick LR. **2001**. Restionaceae seedlings: Morphology, anatomy and systematic implications. *Feddes Repertorium* **112**: 59–80.

Linder HP, Vlok JH. **1991**. The morphology, taxonomy and evolution ofRhodocoma (Restionaceae). *Plant Systematics and Evolution* **175**: 139–160.

Lloyd DG. **1984**. Variation strategies of plants in heterogeneous environments. *Biological Journal of the Linnean Society* **21**: 357–385.

Makino A, Mae T, Ohira K. **1985**. Photosynthesis and ribulose-1,5-bisphosphate carboxylase/oxygenase in rice leaves from emergence through senescence. Quantitative analysis by carboxylation/oxygenation and regeneration of ribulose 1,5-bisphosphate. *Planta* **166**: 414–420.

Mappin KA, Pate JS, Bell TL. **2003**. Productivity and water relations of burnt and long-unburnt semi-arid shrubland in Western Australia. *Plant and Soil* **257**: 321–340.

McGill BJ, Enquist BJ, Weiher E, Westoby M. **2006**. Rebuilding community ecology from functional traits. *Trends in Ecology & Evolution* **21**: 178–185.

Miller PM, Eddleman LE, Miller JM. **1995**. *Juniperus occidentalis* juvenile foliage: advantages and disadvantages for a stress-tolerant, invasive conifer. *Canadian Journal of Forest Research* **25**: 470–479.

Moreno JM, Oechel WC. **2012**. *The Role of Fire in Mediterranean-Type Ecosystems*. Springer Science & Business Media.

Morris TL, Esler KJ, Barger NN, Jacobs SM, Cramer MD. **2011**. Ecophysiological traits associated with the competitive ability of invasive Australian acacias. *Diversity and Distributions* **17**: 898–910.

Mueller-Dombois D, Fosberg FR. **1998**. *Vegetation of the Tropical Pacific Islands*. New York: Springer.

Murphy DJ, Miller JT, Bayer RJ, Ladiges PY. **2003**. Molecular phylogeny of *Acacia* subgenus *Phyllodineae* (Mimosoideae : Leguminosae) based on DNA sequences of the internal transcribed spacer region. *Australian Systematic Botany* **16**: 19–26.

Myers N, Mittermeier RA, Mittermeier CG, da Fonseca GAB, Kent J. **2000**. Biodiversity hotspots for conservation priorities. *Nature* **403**: 853–858.

Pabón-Mora N, González F. **2012**. Leaf Development, Metamorphic Heteroblasty and Heterophylly in Berberis s. l. (Berberidaceae). *The Botanical Review* **78**: 463–489.

Parra A, Moreno JM. **2017**. Post-fire environments are favourable for plant functioning of seeder and resprouter Mediterranean shrubs, even under drought. *The New Phytologist* **214**: 1118–1131.

Pérez-Ramos IM, Roumet C, Cruz P, Blanchard A, Autran P, Garnier E. **2012**. Evidence for a 'plant community economics spectrum' driven by nutrient and water limitations in a Mediterranean rangeland of southern France. *Journal of Ecology* **100**: 1315–1327.

Pierce S, Negreiros D, Cerabolini BEL, *et al.* 2016. A global method for calculating plant CSR ecological strategies applied across biomes world-wide. *Functional Ecology*: 444–457.

Pierret A, Gonkhamdee S, Jourdan C, Maeght J-L. **2013**. IJ_Rhizo: an open-source software to measure scanned images of root samples. *Plant and Soil* **373**: 531–539.

Pons TL, Welschen R a. M. **2002**. Overestimation of respiration rates in commercially available clamp-on leaf chambers. Complications with measurement of net photosynthesis. *Plant, Cell & Environment* **25**: 1367–1372.

Poorter H, Niinemets Ü, Poorter L, Wright IJ, Villar R. **2009**. Causes and consequences of variation in leaf mass per area (LMA): a meta-analysis. *New Phytologist* **182**: 565–588.

Rao CV. **1971**. *Proteaceae*. New Delhi: Council of Scientific & Industrial Research.

Rebelo AG, Boucher C, Helme N, Mucina L. **2006**. Fynbos Biome In: Mucina L, Rutherford MC, eds. *The vegetation of South Africa, Lesotho and Swaziland*. South African National Biodiversity Institute, 53–219.

Reich PB. **2014**. The world-wide 'fast–slow' plant economics spectrum: a traits manifesto. *Journal of Ecology* **102**: 275–301.

Reich PB, Ellsworth DS, Walters MB, *et al.* 1999. Generality of Leaf Trait Relationships: A Test Across Six Biomes. *Ecology* **80**: 1955–1969.

Reich PB, Walters MB, Ellsworth DS. **1997**. From tropics to tundra: Global convergence in plant functioning. *Proceedings of the National Academy of Sciences* **94**: 13730–13734.

Scott DF, Wyk DB van. **1992**. The Effects of Fire on Soil Water Repellency, Catchment Sediment Yields and Streamflow In: Ecological Studies. *Fire in South African Mountain Fynbos*. Springer, Berlin, Heidelberg, 216–239.

Silvertown J, Araya YN, Linder HP, Gowing DJ. **2012**. Experimental investigation of the origin of fynbos plant community structure after fire. *Annals of Botany* **110**: 1377–1383.

Stock WD, Lewis OAM. **1986**. Soil Nitrogen and the Role of Fire as a Mineralizing Agent in a South African Coastal Fynbos Ecosystem. *Journal of Ecology* **74**: 317–328.

Stock WD, Sommerville JEM, Lewis O a. M. **1987**. Seasonal allocation of dry mass and nitrogen in a fynbos endemic Restionaceae species Thamnochortus punctatus Pill. *Oecologia* **72**: 315–320.

Vile D, Shipley B, Garnier E. **2006**. A structural equation model to integrate changes in functional strategies during old-field succession. *Ecology* **87**: 504–517.

Westoby M, Wright IJ. **2006**. Land-plant ecology on the basis of functional traits. *Trends in Ecology & Evolution* **21**: 261–268.

Wright IJ, Reich PB, Westoby M, *et al.* 2004. The worldwide leaf economics spectrum. *Nature* **428**: 821–827.

Zotz G, Wilhelm K, Becker A. **2011**. Heteroblasty—A Review. *Botanical Review* **77**: 109–151.

Supplement

Supplementary information 1: Extension of the niche overlap method of Broennimann et al. (2012)

We present a method of calculating overlaps (niche, traits or other) in multidimensional space based on relative frequency along *n*-dimensional variable gradients (Fig S1). The data required for this approach is presence data of two subjects under variables of interest (e.g. occurrence of species under environmental conditions such as temperature, rainfall and seasonality or individuals of two populations in trait space).

This multidimensional space in which the occurrences are placed in order to estimate occurrence probabilities can be defined as either a "global" setup (e.g. such as a climate of a whole region) or as the combined range of the two subjects to be compared (e.g. the dataset of climatic conditions of all occurrences of a population that is invasive combined with the climatic conditions of the occurrences in its native distribution), thus allowing for different background and reference systems.

This reference space is then evenly binned by slicing all number of j dimensions into n bins, resulting in a multivariate binned cell space, with each cell representing a different combination of binned values of the dimensions.

To calculate the overlap between subjects in that reference space, we assign to each cell an occurrence probability (i.e. the probability of being present in that particular cell) for each subject separately.

We implement a way of correcting for unequal presence of certain conditions in the reference system represented by the cells (e.g. more or less common environmental conditions in a region, which translate in a higher or lower change of species being present in the frequent or rare habitats by chance) In this case, the relative frequency of each cell in the reference system is assigned to the each cell, and the subjects occurrence probability in a condition represented by a cell is divided by the relative frequency of this cell. This results in an occurrence probability for each cell regardless of how rare the conditions of the cell are in the background (e.g. interpretable as the chance to find a member of the species analysed in a site resembling the conditions of a specific cell, or in numbers: a species occurs in 5 sites with a certain condition (or 5% of all of that species' occurrences are in that condition); such sites with that condition exist 10 times in a certain region (or 10% of all sites in the region); thus the probability to find an individual of that species in that environment is 0.5).

The occurrence probabilities for a subject for all cells (after being corrected for the frequencies) get normalized to the sum of 1 (which is interpretable as if one occurrence of a subject were randomly drawn, which condition (which cell) would it be from, thus resembling the chances of the condition the occurrence is sampled from).

The normalized grid cell probabilities of the two subjects are then used for calculating Warren's I (Warren *et al.*, 2008) or Schoener's D (Schoener, 1965) niche overlap indices, by comparing the chances of the two subject sharing cells, and to which degree.

These occurrence probabilities/relative frequencies can be estimated either using a multidimensional density kernel or by the multiplication of the grid cells' single dimension's occurrence probability/ relative frequency estimated by single dimension density estimation, depending on the user's choice and available computational power.

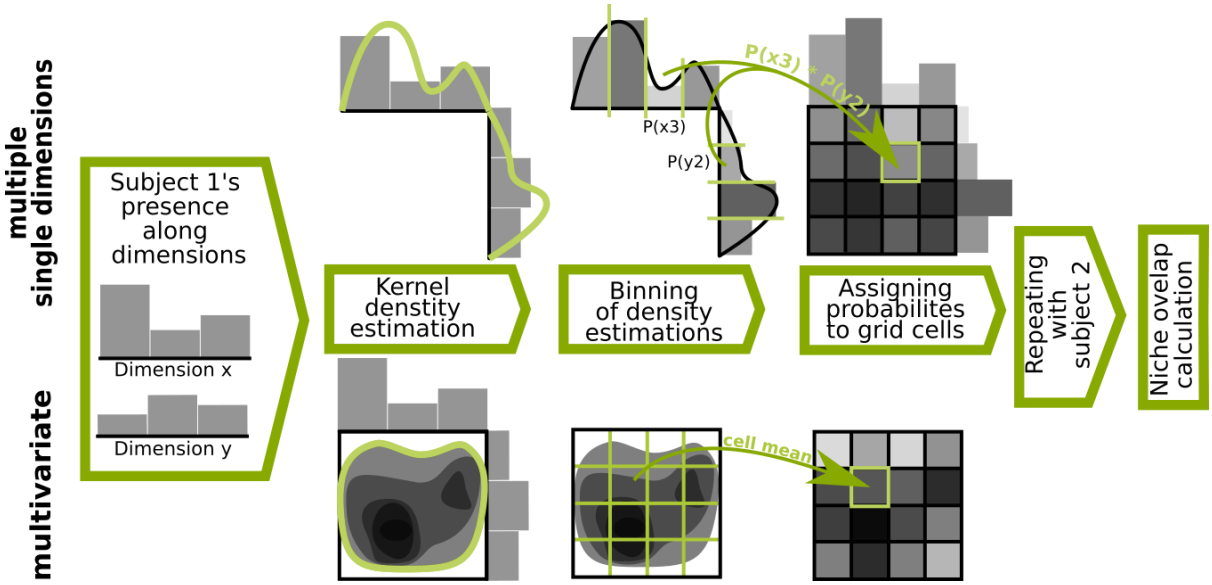

Fig. S1. Framework for calculating the species niches from multidimensional data, using multiple single dimension kernel density estimations (top) or applying a multivariate kernel density estimation (bottom).

The density kernel implemented here (function kde, package ks) (Duong, 2017) allows up to 6 dimensions and could be easily modified to allow any independent number of bins for each dimension, though this is currently not implemented. The density kernel used by Broenniman et al.(2012) only allows for 2 dimensions and always requires an equal bin number on all dimension. Multivariate kernel density estimation is computationally intense and may take more time. The single density multiplication method is not restricted in the number of dimensions and it is computationally much less intense, allowing for faster computation. Both methods however are limited by available memory space, due to the necessary creation of

matrices with the length of number of bins n to the power of number of used dimensions j, n^j. Both ways lead to very similar niche overlap values when tested (Fig. S2). While the single dimension multiplication method is more conservative (if a subject has zero probability in certain bins along one dimension, the subject will not be present in any cells with this binned value on this dimension at all, regardless of potentially high probabilities on other dimensions), this assumption is relaxed by multidimensional kernel density estimation.

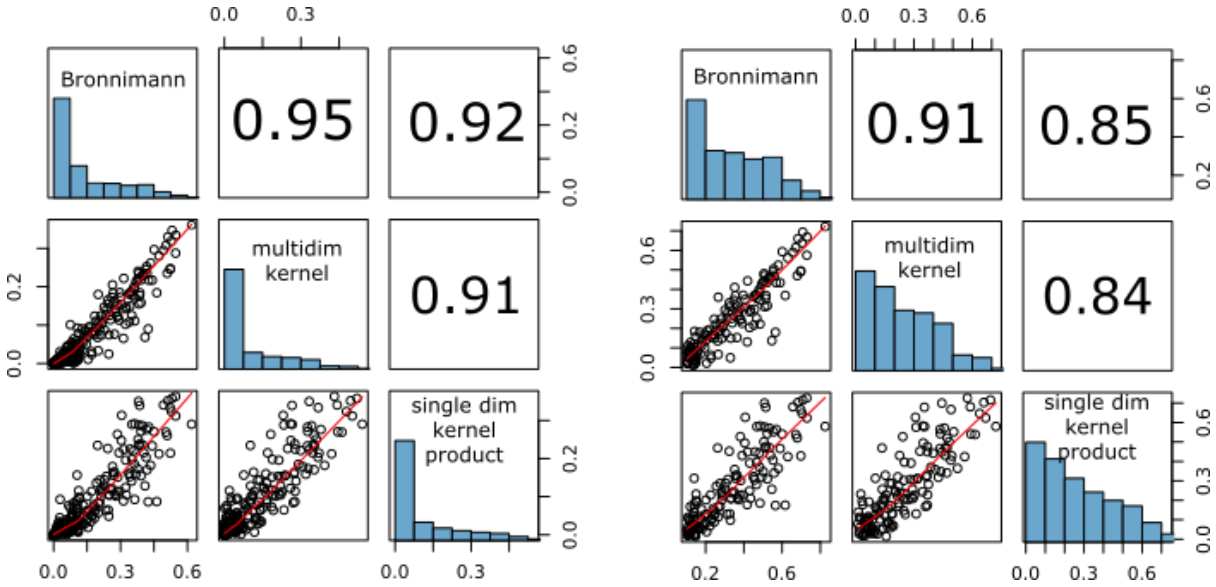

Fig. S2. Pairwise correlation matrix of two-dimensional niche overlap measures derived from the different niche computation methods using 300 random species pairs (left panel) and a subset of where overlaps = 0 were removed (right panel), based on the species occurrences' PC scores, with correction for the global environment and 50 bins per dimension. From top to bottom and left to right the Broenniman et al. (2012) method based on kernelUD function, the multidimensional kernel density estimation method and the single dimension multiplication method. The upper right half of the matrix shows the Pearson correlation coefficient. The lower half shows a scatter plot of the respective niche overlaps and histogram of the overlap distribution in the center.

In our study, we applied this function, using the single dimension multiplication method on three-dimensional data from multivariate ordinations and R = 50 and a global space correction of the respective data sets described in the material and methods sections.

Supplementary information 2: Calculation of species weighted mean environments.

For the phylogenetic generalized logistic models, we used the weighted means of species occurrence probabilities that are corrected by the relative frequency of environmental conditions. Both the occurrence probabilities and the relative frequencies were estimated using single kernel density estimation, similar to the correction used for the niche-overlap calculations. For each species, its occurrence probability density along each ordination axis is

computed, and likewise for each respective ordination axis the relative frequency of the conditions in the reference system is estimated using all sites (all regional grid cells' conditions of the climate PCA; all plots' habitat conditions of the local habitat PCoA). The species and reference system densities are binned into 500 equal sections. The species binned densities get divided by the reference system's binned densities. In case of a division by 0, the species probability in the specific environment bin is defined as 0 as well. The 500 corrected species densities then get normalized to the sum of 1, representing species probabilities in each of the 500 bins. These species probabilities are then used to calculate a weighted mean of the respective 500 binned ordination scores that represent in our case the climatic (using the regional grid cell climatic PCA) or habitat conditions (using the plot-based habitat PCoA).
Our corrected mean calculation function also allows for and can sample a set number of values (bins) by the corrected species probability, or from a predefined centred quantile (such as the inner 95% of the species).

Supplementary information 3: Model of abundance of neotenous species in local habitat conditions.

Material and method

To assess whether neotenous species are more frequent in some environments than others, we used a dataset of 934 plots reporting presence of restio species and categorical descriptions of local habitat conditions. We excluded all species with fewer than three occurrences, leaving 888 plots with a total of 4187 occurrence records for 233 species. We ordered the categorical descriptors (apart from soil depth, which was already ordered) and interpreted the bedrock type as degree of fertility according to (Bradshaw & Cowling, 2014), thus generating a set of ordered factors in addition to the categorical data (Table S1).
We then generated a data matrix of plots with their ordered and categorical descriptors and added all species present in respective plots with the respective plots' descriptors. This combined plot and species-in-plots dataset was used to calculate a Gower dissimilarity matrix. Based on that dissimilarity matrix, we computed a PCoA, weighting the species 0 and the plots 1: in this way, the PCoA space is entirely defined by the plots – irrespective of the number of species in each plot, but we were able to easily extract the scores of the included- but unweighted species present in their respective plots.
After extracting PCoA scores of the most informative axes for the of all species present in plot, we calculated species weighted mean scores, with weights representing the relative frequency

of species in their habitats given by plots, corrected for the frequency of respective habitat conditions: for example, if a species occurs 3 times in plots with conditions that were sampled only 4 times, its abundance probability in these conditions is 0.75; in contrast, a species being present in 10 plots with a more common condition that was sampled 30 times gets an occurrence probability of 33% in such habitat. The species' "preference", and thus weighted mean, is shifted towards the rare condition. To compute the weighted means we used the same method applied to the climatic PCA scores, described in supplementary information 2. We proceeded with phylogenetic logistic models using a pruned tree, including only the species present in the plot dataset. We then modelled the probability of abundance of neotenic species along PCoA axes reflecting habitat condition, similar to as described for the climate PCA analysis.

Table S1. Habitat data descriptors used as categorical variables together with their ordered states used to calculate a Gower distance to compute the plot-based habitat PCoA

Habitat descriptor	Factor state	Ordered state
Bedrock/soil type (degree of fertility)	Sandstone	1
	Acidic sand	
	Granite	2
	Laterite	
	Sand	
	Quartzite	
	Shale	3
	Tillite	4
	Recent sand	
	Silcrete	
	Limestone	5
Soil water condition	Well-drained	1
	Seep	2
	Impeded drainage	
	Cliff-seep	
	Convex-seep	
	Valley-bottom	
	Marsh	3
	Streambank	4
Rockiness	None	1
	Pebbles	2
	Pebbles/boulders	3
	Boulders	4
	Pebbles/boulders/bedrock	
	Cliffs	5

	Bedrock	
Soil texture	Sand	1
	Organic/sand	2
	Sandy loam	2
	Loam	3
	Organic	
	Loamy clay	4
	Clay	5

Results

Using the plot based PCoA scores based on local habitat conditions, we found a significant relationship between PCoA axes 1 and 5 and the presence probability of retaining species (both: $P < 0.05$, Table S9). PCoA axis 1 is negatively correlated with soil depth and texture and weakly with bedrock type fertility, and positively with rockiness (Figs 5 and S3). PCoA axis 1 explains 25.53% of the variance. PCoA axis 5 is negatively correlated with habitat wetness and weakly with bedrock type fertility and explains 7.0% of the plot's conditions variance.

The z-values of PCoA axes 1 and 5 of the logistic model is outside the 95% quantiles of the z-values of models built for randomized trait group assignments (Fig. S5), thus, retaining species are not randomly distributed across the environmental variation of the plots. The test for topological uncertainty however shows some susceptibility to phylogenetic uncertainty particularly for PCoA axis 5 (Fig. S8).

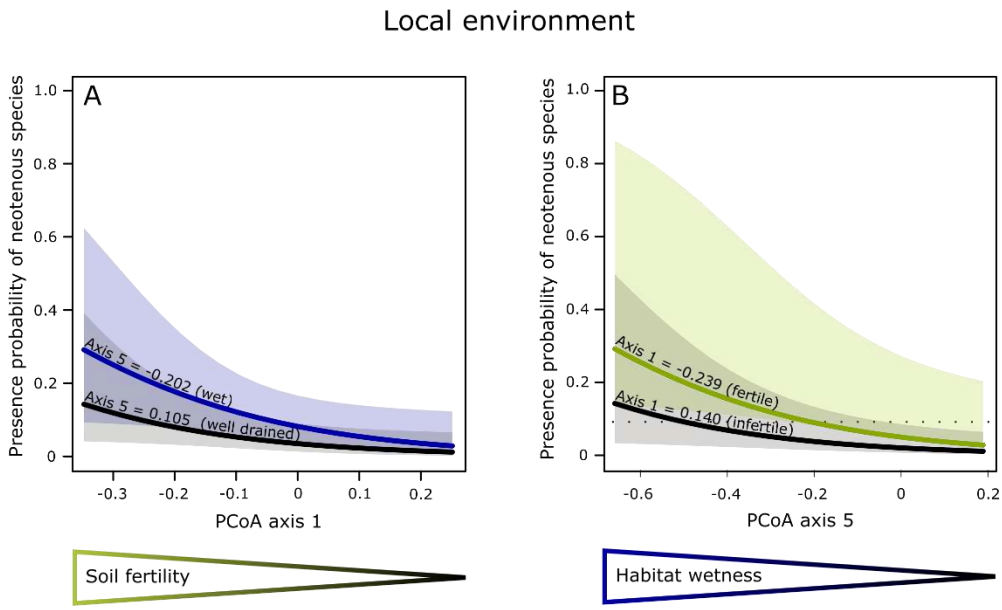

Fig. S3. Multivariate phylogenetic logistic models predicting the probability of presence of retaining restio species along local environmental gradients. The gradients are represented by axis 1 of the PCoA based on categorical and ordinal habitat descriptors that correlates with soil depth and texture and weakly bedrock type fertility (A), and axis 5 correlating with habitat wetness (B). The two curves in each graph reflect the 90%ile (coloured curves) and 10%ile (black curves) values of the second significant predictor of the model. The shaded area represents the 95% confidence intervals. The dotted line represents the expected probability of presence of retaining species under the null model. The non-significant predictors (axes 2- 4) were fixed using their medians.

Supplementary References

Bradshaw PL, Cowling RM. **2014**. Landscapes, rock types, and climate of the Greater Cape Floristic Region. In: Allsopp N, Colville JF, Verboom GA, eds. Fynbos. Oxford University Press, 26–46.

Duong T. **2017**. *ks: Kernel Smoothing*.

Schoener TW. **1965**. The Evolution of Bill Size Differences Among Sympatric Congeneric Species of Birds. *Evolution* **19**: 189–213.

Warren DL, Glor RE, Turelli M, Funk D. **2008**. Environmental Niche Equivalency versus Conservatism: Quantitative Approaches to Niche Evolution. *Evolution* **62**: 2868–2883.

Supplementary Figures

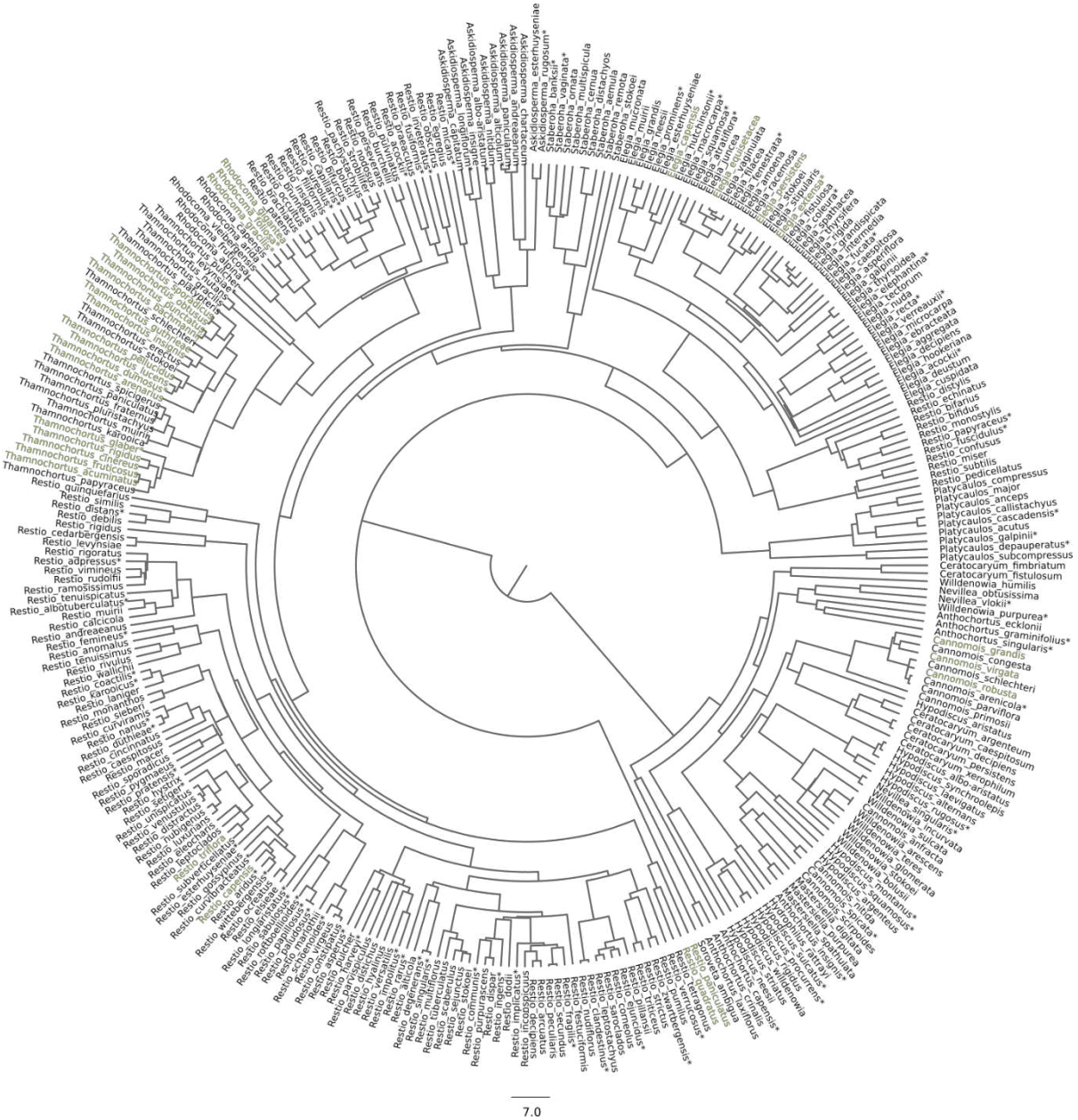

Fig. S4. Phylogenetic tree of all Restionaceae species included in our study. Species in green are species with adult sterile shoots. Species with asterisk (*) are not included in the plot-based analysis.

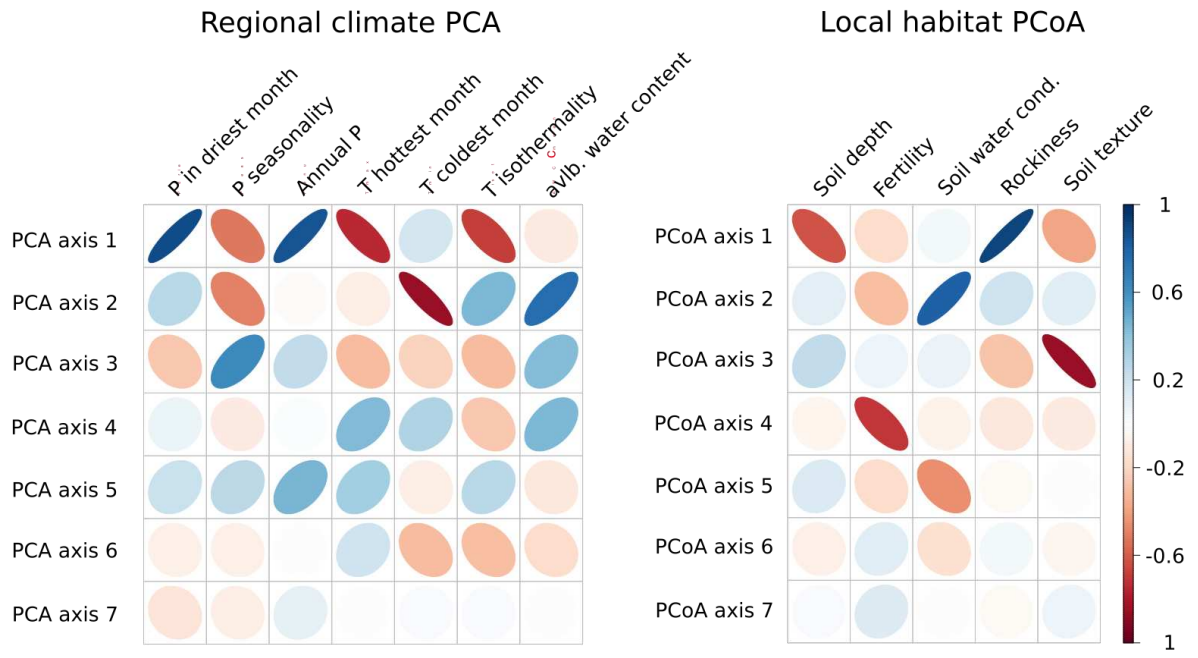

Fig. S5. Correlation matrix plots of PCA axes with environmental variables (left) and PCoA axes with the ordered habitat conditions (right). P stands for precipitation, T for temperature. Correlation strength and direction is visualized by shape and colour: ascending narrow dark blue ellipses indicate positive correlation; descending, narrow, red ellipses indicate negative correlation.

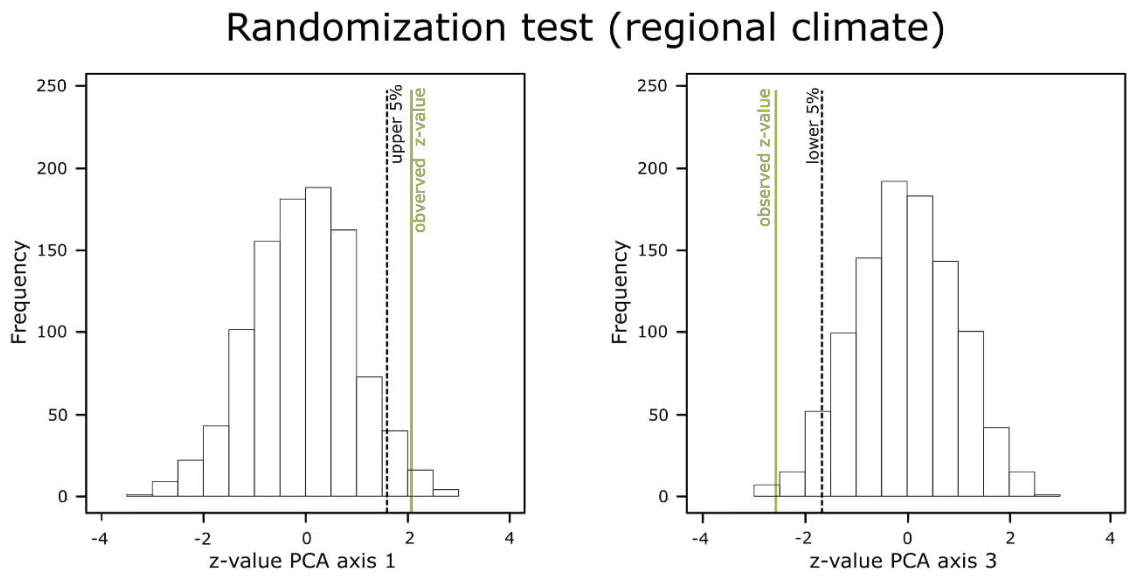

Fig. S6. Histograms of z-values of phylogenetic logistic models of predicting retaining restio occurrence probabilities by regional climate PCA axes with randomized species' characteristic of presence of adult sterile shoots in contrast to observed z-value (green).

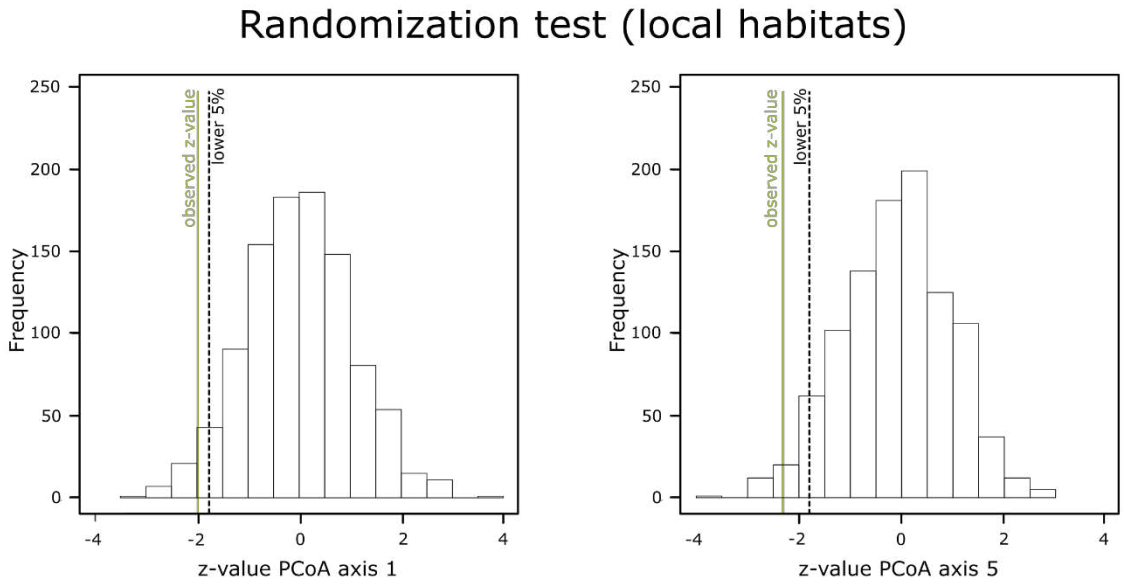

Fig. S7. Histograms of z-values of phylogenetic logistic models of predicting retaining restio occurrence probabilities by local habitat PCoA axes with randomized species' characteristic of presence of adult sterile shoots in contrast to observed z-value (green).

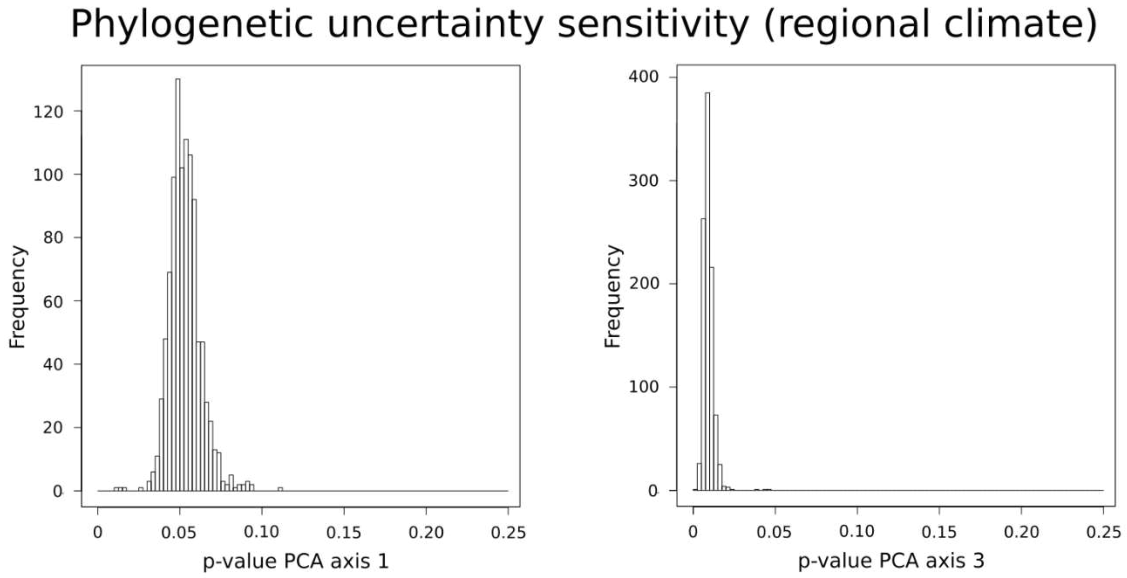

Fig. S8. Histograms of probability values (p-values) for the phylogenetic logistic model‘s null hypothesis (no climatic effect on the presence of retaining species) being true using 1000 randomly sampled post-burnin trees for phylogenetic correction.

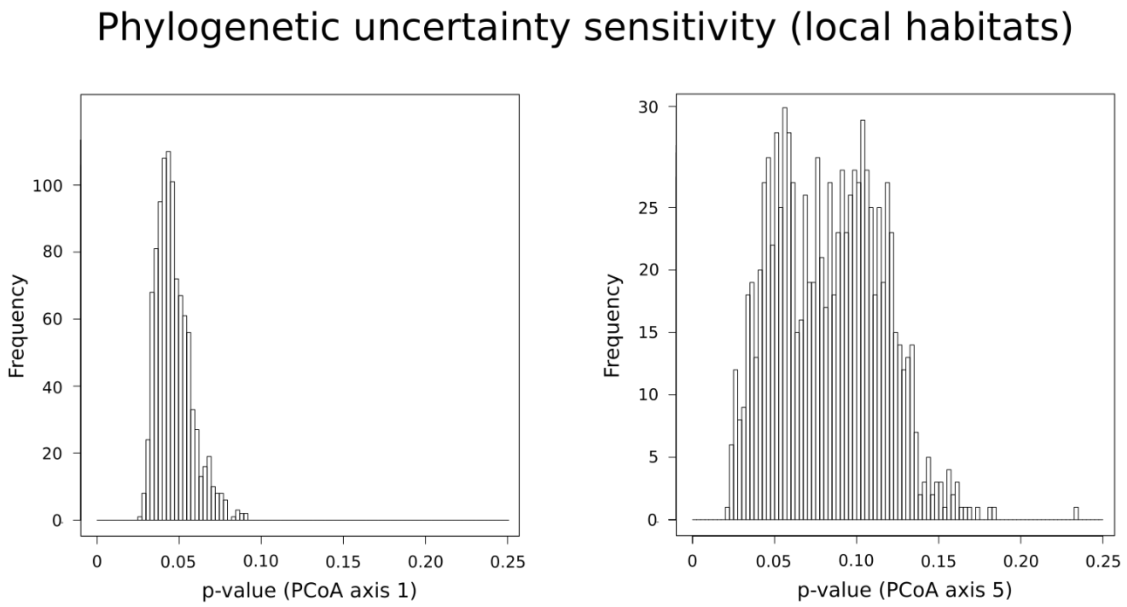

Fig. S 9. Histograms of probability values (p-values) for the phylogenetic logistic model‘s null hypothesis (no local environment effect on the presence of retaining species) being true using 1000 randomly sampled post-burnin trees for phylogenetic correction.

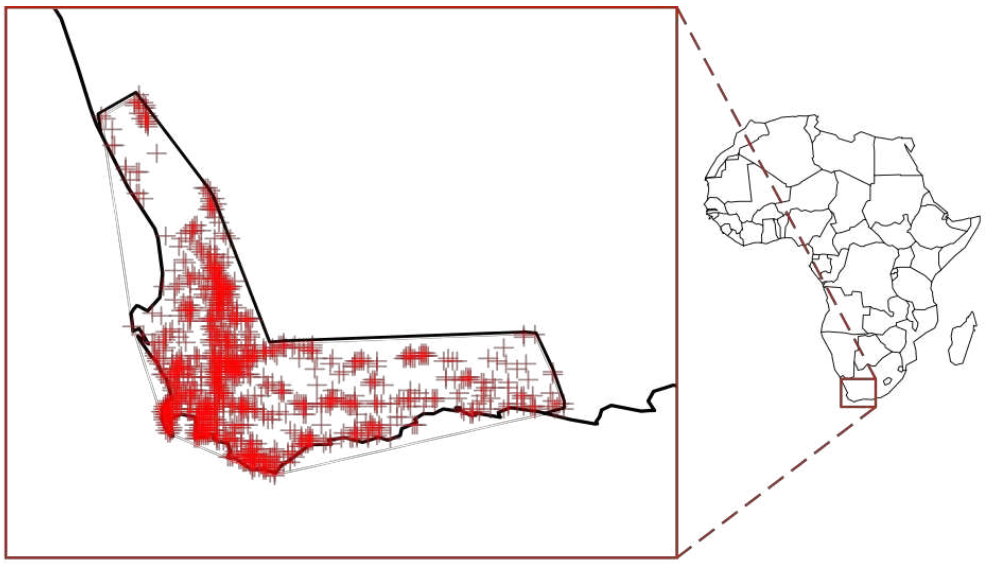

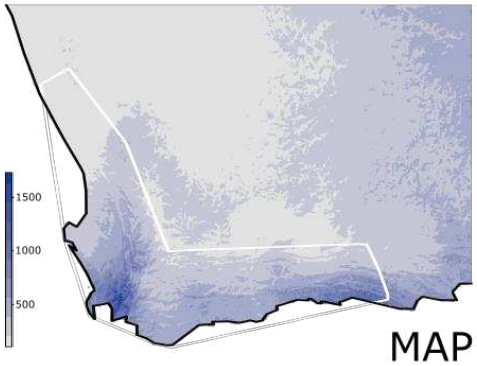
1500
1000
500
MAP

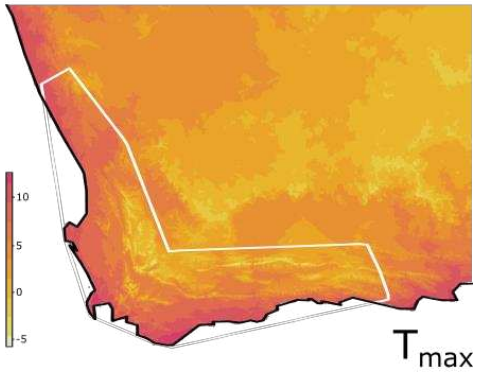
10
5
0
-5
T_{max}

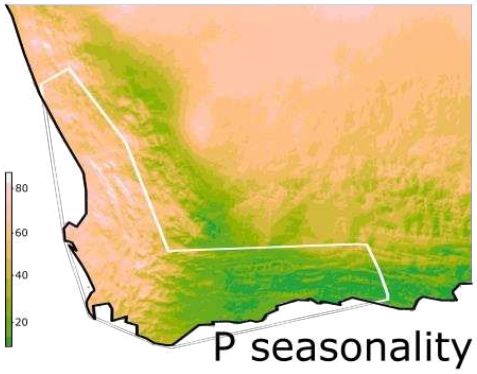
80
60
40
20
P seasonality

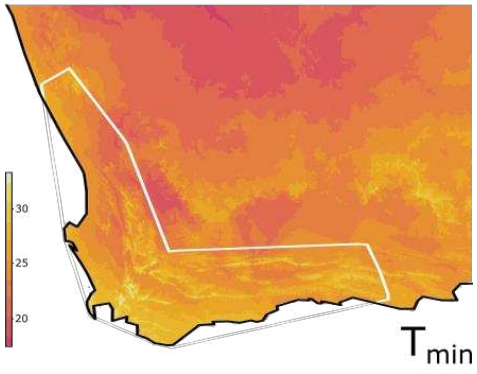
30
25
20
T_{min}

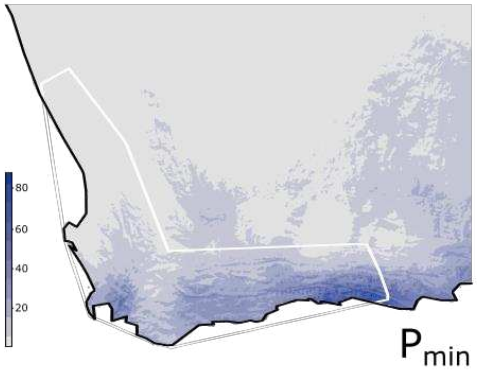
80
60
40
20
P_{min}

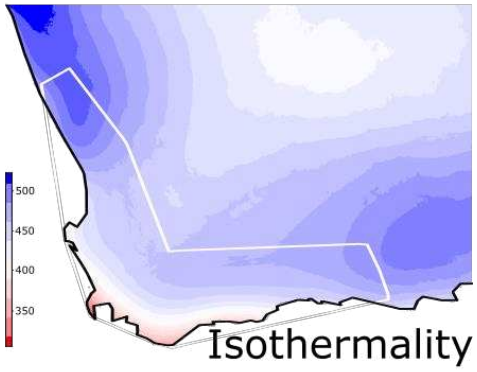
500
450
400
350
Isothermality

Fig. S 10. Occurrence points in the Cape region (red crosses), with polygon defining the region(black) (top); climate model raster maps of variables used. MAP, mean annual precipitation [mm]; P seasonality, precipitation seasonality (Standard deviation of mean monthly precipitation/mean monthly precipitation); P_{min}, mean Precipitation in the driest month [mm]; T_{max}, mean temperature in the hottest month [°C]; T_{min}, mean temperature in the coldest month [°C], Isothermality, (mean monthly difference of maximum and minimum Temperature/T_{max}-T_{min})*100.

Supplementary Tables

Table S2. Model coefficients of the linear mixed effects model (SMA ~ shoot type) with nested random effects of individual in species. Statistical significance codes: *** p < 0.001.

	Estimate	Standard error	Degrees of freedom	t value	p-value	
(Intercept)	0.192	0.012	15.640	15.46	0.192	***
shoot type (sterile)	-0.145	0.008	146.42	-17.78	-0.145	***

Table S3 Model coefficients of the linear mixed effects model (A_{mass} ~ shoot type) with nested random effects of individual in species. Statistical significance codes: ** p < 0.01, *** p < 0.001.

	Estimate	Standard error	df	t value	p-value	
(Intercept)	0.510	0.071	12.020	7.202	0.001	**
shoot type (sterile)	0.530	0.065	130.55	8.069	<0.001	***

Table S4. Model coefficients of the linear mixed effects model (CSR ~ shoot type) with nested random effects of individual in species. Statistical significance codes: *** p < 0.001.

	Estimate	Standard error	Degrees of freedom	t value	p-value	
(Intercept)	0.206	0.051	20.280	4.018	>0.001	***
shoot type (sterile)	0.720	0.057	40.190	12.532	>0.001	***

Table S5. Posthoc pairwise Differences of Least Squares Means (population means) table of the model trait distance within species~ shoot types compared with nested random effects of individual in species. Statistical significance code: *** p < 0.001; ** p <0.01; *, p < 0.05. D, Euclidean distance; neot, adult sterile (neotenous) shoots; sterile, juvenile sterile shoots; repr, reproductive shoots.

Compared groups	Mean difference	Standard Error	Degrees of freedom	t-value	Lower CI	Upper CI	p-value
$D_{neot\ sterile}$ - $D_{within\ neot}$	0.4	0.1474	109	2.72	0.1089	0.693	<0.01**
$D_{neot\ sterile}$ - $D_{neot\ repr}$	-0.3	0.1156	109	-2.28	-0.4925	-0.0343	<0.05*
$D_{neot\ sterile}$ - $D_{within\ repr}$	0.7	0.1474	109	4.92	0.4326	1.0168	<0.001***

$D_{neot\ sterile}$ - $D_{repr\ sterile}$	-0.4	0.1156	109	-3.55	-0.64	-0.1818	<0.001***
$D_{neot\ sterile}$ - $D_{within\ sterile}$	0.3	0.1474	109	2.36	0.0557	0.6398	<0.05*
$D_{within\ neot}$ - $D_{neot\ repr}$	-0.7	0.1474	109	-4.51	-0.9564	-0.3723	<0.001***
$D_{within\ neot}$ – $D_{within\ repr}$	0.3	0.1734	109	1.87	-0.0199	0.6674	0.065
$D_{within\ neot}$ - $D_{repr\ sterile}$	-0.8	0.1474	109	-5.51	-1.1039	-0.5198	<0.001***
$D_{within\ neot}$ - $D_{within\ sterile}$	-0.1	0.1734	109	-0.31	-0.3969	0.2905	0.76
$D_{neot\ repr}$ - $D_{within\ repr}$	1	0.1474	109	6.71	0.6961	1.2802	<0.001***
$D_{neot\ repr}$ - $D_{repr\ sterile}$	-0.1	0.1156	109	-1.28	-0.3766	0.0817	0.205
$D_{neot\ repr}$ - $D_{within\ sterile}$	0.6	0.1474	109	4.15	0.3191	0.9032	<0.001***
$D_{within\ repr}$ - $D_{repr\ sterile}$	-1.1	0.1474	109	-7.71	-1.4277	-0.8435	<0.001***
$D_{within\ repr}$ - $D_{within\ sterile}$	-0.4	0.1734	109	-2.17	-0.7206	-0.0333	<0.05*
$D_{repr\ sterile}$ - $D_{within\ sterile}$	0.8	0.1474	109	5.15	0.4666	1.0507	<0.001***

Table S6. Model coefficients of the phylogenetic logistic model (pres. of adult sterile shoots ~ PCA axis 1 + PCA axis 2 + PCA axis 3, using IG10 method. The Wald-type p-values for the coefficients are conditional on alpha=0.124. Statistical significance codes: *** p < 0.001, ** p < 0.01, * p < 0.05.

	Estimate	Standard error	z-value	p-value	
(Intercept)	-2.683	0.537	-5.001	<0.001	***
PCA axis 1	0.326	0.157	2.076	0.038	*
PCA axis 2	0.042	0.092	0.454	0.650	
PCA axis 3	-0.451	0.175	-2.585	0.010	**

Table S7. Regional climate PCA variable loadings. P stands for precipitation, T stands for temperature.

	P in driest month	P seasonality	Annual P	T in hottest month	T in coldest Month	T isothermality	Mean annual water content
PCA axis 1	0.522	-0.310	0.503	-0.443	0.109	-0.407	-0.064
PCA axis 2	0.199	-0.368	-0.012	-0.061	-0.633	0.329	0.558
PCA axis 3	-0.279	0.646	0.254	-0.315	-0.220	-0.320	0.436
PCA axis 4	0.104	-0.128	0.024	0.580	0.390	-0.359	0.596
PCA axis 5	0.298	0.358	0.626	0.468	-0.119	0.366	-0.157
PCA axis 6	-0.152	-0.151	0.016	0.381	-0.597	-0.582	-0.337
PCA axis 7	-0.698	-0.429	0.538	-0.019	0.127	0.147	0.032

Table S8. Correlation matrix of regional climate PCA axes and climatic variables. P stands for precipitation, T stands for temperature.

	P in driest month	P seasonality	Annual P	T in hottest month	T in coldest Month	T isothermality	Mean annual water content
PCA axis 1	0.882	-0.524	0.850	-0.748	0.184	-0.688	-0.109
PCA axis 2	0.270	-0.498	-0.016	-0.082	-0.857	0.446	0.755

PCA axis 3	-0.269	0.623	0.245	-0.304	-0.213	-0.309	0.420
PCA axis 4	0.078	-0.096	0.018	0.433	0.291	-0.268	0.445
PCA axis 5	0.216	0.260	0.454	0.339	-0.086	0.266	-0.114
PCA axis 6	-0.078	-0.077	0.008	0.195	-0.306	-0.298	-0.173
PCA axis 7	-0.133	-0.082	0.103	-0.004	0.024	0.028	0.006

Table S9. Regional climate PCA axes' eigenvalues and explained variance. P stands for precipitation, T stands for temperature.

	Eigenvalues	% explained variance	Cumulative % explained variance
PCA axis 1	431637.680	40.790	40.790
PCA axis 2	276915.990	26.168	66.958
PCA axis 3	140692.360	13.295	80.254
PCA axis 4	84285.840	7.965	88.219
PCA axis 5	79467.840	7.510	95.728
PCA axis 6	39702.750	3.752	99.480
PCA axis 7	5501.540	0.520	100.000

Table S10. Model coefficients of the phylogenetic logistic model (pres. of adult sterile shoots ~ PCoA axis 1 + … + PCoA axis 5, using IG10 method. The Wald-type p-values for the coefficients are conditional on alpha=0.097.. Statistical significance codes: *** p < 0.001, * p < 0.05.

	Estimate	Standard error	z-value	p value	
Intercept	-3.007	0.437	-6.875	0.000	***
PCoA Axis 1	-4.429	2.175	-2.037	0.042	*
PCoA Axis 2	-0.345	1.544	-0.223	0.823	
PCoA Axis 3	-2.797	2.170	-1.289	0.198	
PCoA Axis 4	-0.286	2.018	-0.142	0.887	
PCoA Axis 5	-3.037	1.306	-2.325	0.020	*

Table S11. Local habitat PCoA Axis eigenvalues and explained variance.

	Eigenvalues	% explained variance	cumulative % explained variance
PCoA Axis 1	3.502E-02	25.542	25.542
PCoA Axis 2	2.959E-02	21.581	47.123
PCoA Axis 3	2.197E-02	16.027	63.150
PCoA Axis 4	1.418E-02	10.344	73.494
PCoA Axis 5	9.635E-03	7.028	80.523
PCoA Axis 6	5.692E-03	4.152	84.675
PCoA Axis 7	3.387E-03	2.470	87.146
PCoA Axis 8	2.933E-03	2.140	89.285

PCoA Axis 9	2.591E-03	1.890	91.176
PCoA Axis 10	2.490E-03	1.817	92.992
PCoA Axis 11	1.438E-03	1.049	94.041
PCoA Axis 12	1.322E-03	0.965	95.006
PCoA Axis 13	1.080E-03	0.788	95.794
PCoA Axis 14	9.749E-04	0.711	96.505
PCoA Axis 15	9.285E-04	0.677	97.182
PCoA Axis 16	8.149E-04	0.594	97.777
PCoA Axis 17	6.708E-04	0.489	98.266
PCoA Axis 18	6.281E-04	0.458	98.724
PCoA Axis 19	4.639E-04	0.338	99.063
PCoA Axis 20	3.909E-04	0.285	99.348
PCoA Axis 21	3.257E-04	0.238	99.585
PCoA Axis 22	2.341E-04	0.171	99.756
PCoA Axis 23	9.277E-05	0.068	99.824
PCoA Axis 24	7.293E-05	0.053	99.877
PCoA Axis 25	6.518E-05	0.048	99.925
PCoA Axis 26	5.176E-05	0.038	99.962
PCoA Axis 27	3.144E-05	0.023	99.985
PCoA Axis 28	1.478E-05	0.011	99.996
PCoA Axis 29	5.421E-06	0.004	100.000

Table S12. Correlation matrix of PCoA Axis with ordinal scored habitat variables.

	Soil depth	Fertility	Soil water condition	Rockiness	Soils type
PCoA Axis 1	-0.628	-0.177	0.040	0.911	-0.382
PCoA Axis 2	0.110	-0.299	0.801	0.200	0.127
PCoA Axis 3	0.248	0.066	0.081	-0.273	-0.850
PCoA Axis 4	-0.058	-0.702	-0.062	-0.117	-0.109
PCoA Axis 5	0.148	-0.175	-0.452	-0.023	-0.007
PCoA Axis 6	-0.077	0.126	-0.155	0.046	-0.049
PCoA Axis 7	0.026	0.131	-0.008	-0.028	0.065
PCoA Axis 8	-0.025	-0.025	-0.059	-0.020	0.018
PCoA Axis 9	0.004	0.255	0.033	0.034	-0.053
PCoA Axis 10	-0.047	0.273	0.046	0.033	-0.034
PCoA Axis 11	-0.011	-0.075	-0.058	-0.060	-0.018
PCoA Axis 12	0.002	0.023	0.046	0.034	0.051
PCoA Axis 13	-0.031	0.070	-0.018	-0.042	-0.059
PCoA Axis 14	-0.094	0.097	-0.017	-0.036	0.029
PCoA Axis 15	-0.002	0.123	0.051	0.010	-0.046
PCoA Axis 16	0.015	-0.083	-0.015	0.011	0.017
PCoA Axis 17	0.018	0.119	0.019	-0.022	-0.079
PCoA Axis 18	-0.012	-0.043	0.014	0.033	-0.006

PCoA Axis 19	-0.010	-0.176	0.019	0.019	-0.033
PCoA Axis 20	0.033	0.197	-0.003	-0.040	0.127
PCoA Axis 21	-0.008	0.058	0.015	-0.022	0.195
PCoA Axis 22	0.000	0.031	-0.018	-0.004	-0.125
PCoA Axis 23	0.035	0.010	-0.020	-0.064	-0.024
PCoA Axis 24	-0.014	0.023	-0.005	-0.003	0.107
PCoA Axis 25	-0.004	-0.061	0.025	0.032	-0.042
PCoA Axis 26	-0.014	-0.030	0.018	0.041	0.035
PCoA Axis 27	0.010	-0.015	-0.006	0.042	0.005
PCoA Axis 28	-0.049	0.005	0.004	0.000	0.002
PCoA Axis 29	-0.024	-0.004	0.021	-0.035	0.021